Neutrino Mixing

With the exception of the LSND anomaly, current neutrino data can be described within the framework of a 3×3 mixing matrix between the flavor eigenstates ν_e, ν_μ, and ν_τ and the mass eigenstates ν_1, ν_2, and ν_3. (See Eq. (13.31) of the Review "Neutrino Mass, Mixing and Flavor Change" by B. Kayser.) The Listings are divided into the following sections:

(A) Neutrino fluxes and event ratios: shows measurements which correspond to various oscillation tests for Accelerator, Reactor, Atmospheric, and Solar neutrino experiments. Typically ratios involve a measurement in a realm sensitive to oscillations compared to one for which no oscillation effect is expected.

(B) Three neutrino mixing parameters: shows measurements of $\sin^2(2\theta_{12})$, $\sin^2(2\theta_{23})$, Δm^2_{21}, Δm^2_{32}, and limits for $\sin^2(2\theta_{13})$ which are all interpretations of data based on the three neutrino mixing scheme described in the review "Neutrino Mass, Mixing and Flavor Change."

(C) Other neutrino mixing results: shows measurements and limits for the probability of oscillation for experiments which might be relevant to the LSND oscillation claim. Included are experiments which are sensitive to $\nu_\mu \to \nu_e$, $\bar{\nu}_\mu \to \bar{\nu}_e$, sterile neutrinos, and CPT tests.

(A) Neutrino fluxes and event ratios

Events (observed/expected) from accelerator ν_μ experiments.

Some neutrino oscillation experiments compare the flux in two or more detectors. This is usually quoted as the ratio of the event rate in the far detector to the expected rate based on an extrapolation from the near detector in the absence of oscillations.

VALUE	DOCUMENT ID		TECN	COMMENT
• • • We do not use the following data for averages, fits, limits, etc. • • •				
$0.71^{+0.08}_{-0.09}$	[1] ALIU	05	K2K	KEK to Super-K
$0.70^{+0.10}_{-0.11}$	[2] AHN	03	K2K	KEK to Super-K

[1] This ratio is based on the observation of 107 events at the far detector 250 km away from KEK, and an expectation of 151^{+12}_{-10}.

[2] This ratio is based on the observation of 56 events with an expectation of $80.1^{+6.2}_{-5.4}$.

Events (observed/expected) from reactor $\overline{\nu}_e$ experiments.

The quoted values are the ratios of the measured reactor $\overline{\nu}_e$ event rate at the quoted distances, and the rate expected without oscillations. The expected rate is based on the experimental data for the most significant reactor fuels (^{235}U, ^{239}Pu, ^{241}Pu) and on calculations for ^{238}U.

VALUE	*DOCUMENT ID*		*TECN*	*COMMENT*
• • • We do not use the following data for averages, fits, limits, etc. • • •				
$0.658 \pm 0.044 \pm 0.047$	[3] ARAKI	05	KLND	Japanese react. $\sim$ 180 km
$0.611 \pm 0.085 \pm 0.041$	[4] EGUCHI	03	KLND	Japanese react. $\sim$ 180 km
$1.01 \pm 0.024 \pm 0.053$	[5] BOEHM	01		Palo Verde react. 0.75–0.89 km
$1.01 \pm 0.028 \pm 0.027$	[6] APOLLONIO	99	CHOZ	Chooz reactors 1 km
$0.987 \pm 0.006 \pm 0.037$	[7] GREENWOOD	96		Savannah River, 18.2 m
$0.988 \pm 0.004 \pm 0.05$	ACHKAR	95	CNTR	Bugey reactor, 15 m
$0.994 \pm 0.010 \pm 0.05$	ACHKAR	95	CNTR	Bugey reactor, 40 m
$0.915 \pm 0.132 \pm 0.05$	ACHKAR	95	CNTR	Bugey reactor, 95 m
$0.987 \pm 0.014 \pm 0.027$	[8] DECLAIS	94	CNTR	Bugey reactor, 15 m
$0.985 \pm 0.018 \pm 0.034$	KUVSHINN...	91	CNTR	Rovno reactor
$1.05 \pm 0.02 \pm 0.05$	VUILLEUMIER	82		Gösgen reactor
$0.955 \pm 0.035 \pm 0.110$	[9] KWON	81		$\overline{\nu}_e p \rightarrow e^+ n$
0.89 ± 0.15	[9] BOEHM	80		$\overline{\nu}_e p \rightarrow e^+ n$

[3] Updated result of KamLAND, including the data used in EGUCHI 03. Note that the survival probabilities for different periods are not directly comparable because the effective baseline varies with power output of the reactor sources involved, and there were large variations in the reactor power production in Japan in 2003.

[4] EGUCHI 03 observe reactor neutrino disappearance at $\sim$ 180 km baseline to various Japanese nuclear power reactors.

[5] BOEHM 01 search for neutrino oscillations at 0.75 and 0.89 km distance from the Palo Verde reactors.

[6] APOLLONIO 99, APOLLONIO 98 search for neutrino oscillations at 1.1 km fixed distance from Chooz reactors. They use $\overline{\nu}_e p \rightarrow e^+ n$ in Gd-loaded scintillator target. APOLLONIO 99 supersedes APOLLONIO 98. See also APOLLONIO 03 for detailed description.

[7] GREENWOOD 96 search for neutrino oscillations at 18 m and 24 m from the reactor at Savannah River.

[8] DECLAIS 94 result based on integral measurement of neutrons only. Result is ratio of measured cross section to that expected in standard *V-A* theory. Replaced by ACHKAR 95.

[9] KWON 81 represents an analysis of a larger set of data from the same experiment as BOEHM 80.

Atmospheric neutrinos

Neutrinos and antineutrinos produced in the atmosphere induce μ-like and e-like events in underground detectors. The ratio of the numbers of the two kinds of events is defined as μ/e. It has the advantage that systematic effects, such as flux uncertainty, tend to cancel, for both experimental and theoretical values of the ratio. The "ratio of the ratios" of experimental to theoretical μ/e, $R(\mu/e)$, or that of experimental to theoretical μ/total,

$R(\mu/\text{total})$ with total $= \mu+e$, is reported below. If the actual value is not unity, the value obtained in a given experiment may depend on the experimental conditions. In addition, the measured "up-down asymmetry" for μ ($N_{up}(\mu)/N_{down}(\mu)$) or e ($N_{up}(e)/N_{down}(e)$) is reported. The expected "up-down asymmetry" is nearly unity if there is no neutrino oscillation.

R(μ/e) = (Measured Ratio μ/e) / (Expected Ratio μ/e)

VALUE	DOCUMENT ID		TECN	COMMENT
• • • We do not use the following data for averages, fits, limits, etc. • • •				
$0.658 \pm 0.016 \pm 0.035$	[10] ASHIE	05	SKAM	sub-GeV
$0.702^{+0.032}_{-0.030} \pm 0.101$	[11] ASHIE	05	SKAM	multi-GeV
$0.69 \pm 0.10 \pm 0.06$	[12] SANCHEZ	03	SOU2	Calorimeter raw data
	[13] FUKUDA	96B	KAMI	Water Cherenkov
$1.00 \pm 0.15 \pm 0.08$	[14] DAUM	95	FREJ	Calorimeter
$0.60 \ ^{+0.06}_{-0.05} \pm 0.05$	[15] FUKUDA	94	KAMI	sub-GeV
$0.57 \ ^{+0.08}_{-0.07} \pm 0.07$	[16] FUKUDA	94	KAMI	multi-Gev
	[17] BECKER-SZ...	92B	IMB	Water Cherenkov

[10] ASHIE 05 results are based on an exposure of 92 kton yr during the complete Super-Kamiokande I running period. The analyzed data sample consists of fully-contained single-ring e-like events with 0.1 GeV/c $< p_e$ and μ-like events 0.2 GeV/c $< p_\mu$, both having a visible energy $<$ 1.33 GeV. These criteria match the definition used by FUKUDA 94.

[11] ASHIE 05 results are based on an exposure of 92 kton yr during the complete Super-Kamiokande I running period. The analyzed data sample consists of fully-contained single-ring events with visible energy $>$ 1.33 GeV and partially-contained events. All partially-contained events are classified as μ-like.

[12] SANCHEZ 03 result is based on an exposure of 5.9 kton yr, and updates ALLISON 99 result. The analyzed data sample consists of fully-contained e-flavor and μ-flavor events having lepton momentum $>$ 0.3 GeV/c.

[13] FUKUDA 96B studied neutron background in the atmospheric neutrino sample observed in the Kamiokande detector. No evidence for the background contamination was found.

[14] DAUM 95 results are based on an exposure of 2.0 kton yr which includes the data used by BERGER 90B. This ratio is for the contained and semicontained events. DAUM 95 also report $R(\mu/e) = 0.99 \pm 0.13 \pm 0.08$ for the total neutrino induced data sample which includes upward going stopping muons and horizontal muons in addition to the contained and semicontained events.

[15] FUKUDA 94 result is based on an exposure of 7.7 kton yr and updates the HIRATA 92 result. The analyzed data sample consists of fully-contained e-like events with $0.1 < p_e < 1.33$ GeV/c and fully-contained μ-like events with $0.2 < p_\mu < 1.5$ GeV/c.

[16] FUKUDA 94 analyzed the data sample consisting of fully contained events with visible energy $>$ 1.33 GeV and partially contained μ-like events.

[17] BECKER-SZENDY 92B reports the fraction of nonshowering events (mostly muons from atmospheric neutrinos) as $0.36 \pm 0.02 \pm 0.02$, as compared with expected fraction $0.51 \pm 0.01 \pm 0.05$. After cutting the energy range to the Kamiokande limits, BEIER 92 finds $R(\mu/e)$ very close to the Kamiokande value.

R(ν_μ) = (Measured Flux of ν_μ) / (Expected Flux of ν_μ)

VALUE	DOCUMENT ID		TECN	COMMENT
• • • We do not use the following data for averages, fits, limits, etc. • • •				
$0.72 \pm 0.026 \pm 0.13$	[18] AMBROSIO	01	MCRO	upward through-going
$0.57 \pm 0.05 \pm 0.15$	[19] AMBROSIO	00	MCRO	upgoing partially contained
$0.71 \pm 0.05 \pm 0.19$	[20] AMBROSIO	00	MCRO	downgoing partially contained + upgoing stopping
$0.74 \pm 0.036 \pm 0.046$	[21] AMBROSIO	98	MCRO	Streamer tubes
	[22] CASPER	91	IMB	Water Cherenkov
	[23] AGLIETTA	89	NUSX	
0.95 ± 0.22	[24] BOLIEV	81		Baksan
0.62 ± 0.17	CROUCH	78		Case Western/UCI

[18] AMBROSIO 01 result is based on the upward through-going muon tracks with $E_\mu > 1$ GeV. The data came from three different detector configurations, but the statistics is largely dominated by the full detector run, from May 1994 to December 2000. The total live time, normalized to the full detector configuration, is 6.17 years. The first error is the statistical error, the second is the systematic error, dominated by the theoretical error in the predicted flux.

[19] AMBROSIO 00 result is based on the upgoing partially contained event sample. It came from 4.1 live years of data taking with the full detector, from April 1994 to February 1999. The average energy of atmospheric muon neutrinos corresponding to this sample is 4 GeV. The first error is statistical, the second is the systematic error, dominated by the 25% theoretical error in the rate (20% in the flux and 15% in the cross section, added in quadrature). Within statistics, the observed deficit is uniform over the zenith angle.

[20] AMBROSIO 00 result is based on the combined samples of downgoing partially contained events and upgoing stopping events. These two subsamples could not be distinguished due to the lack of timing information. The result came from 4.1 live years of data taking with the full detector, from April 1994 to February 1999. The average energy of atmospheric muon neutrinos corresponding to this sample is 4 GeV. The first error is statistical, the second is the systematic error, dominated by the 25% theoretical error in the rate (20% in the flux and 15% in the cross section, added in quadrature). Within statistics, the observed deficit is uniform over the zenith angle.

[21] AMBROSIO 98 result is for all nadir angles and updates AHLEN 95 result. The lower cutoff on the muon energy is 1 GeV. In addition to the statistical and systematic errors, there is a Monte Carlo flux error (theoretical error) of ± 0.13. With a neutrino oscillation hypothesis, the fit either to the flux or zenith distribution independently yields $\sin^2 2\theta = 1.0$ and $\Delta(m^2) \sim$ a few times 10^{-3} eV^2. However, the fit to the observed zenith distribution gives a maximum probability for χ^2 of only 5% for the best oscillation hypothesis.

[22] CASPER 91 correlates showering/nonshowering signature of single-ring events with parent atmospheric-neutrino flavor. They find nonshowering ($\approx \nu_\mu$ induced) fraction is $0.41 \pm 0.03 \pm 0.02$, as compared with expected 0.51 ± 0.05 (syst).

[23] AGLIETTA 89 finds no evidence for any anomaly in the neutrino flux. They define ρ = (measured number of ν_e's)/(measured number of ν_μ's). They report $\rho(\text{measured}) = \rho(\text{expected}) = 0.96^{+0.32}_{-0.28}$.

[24] From this data BOLIEV 81 obtain the limit $\Delta(m^2) \leq 6 \times 10^{-3}$ eV^2 for maximal mixing, $\nu_\mu \not\rightarrow \nu_\mu$ type oscillation.

R(μ/total) = (Measured Ratio μ/total) / (Expected Ratio μ/total)

VALUE	DOCUMENT ID		TECN	COMMENT
• • • We do not use the following data for averages, fits, limits, etc. • • •				
$1.1^{+0.07}_{-0.12} \pm 0.11$	[25] CLARK	97	IMB	multi-GeV

[25] CLARK 97 obtained this result by an analysis of fully contained and partially contained events in the IMB water-Cherenkov detector with visible energy > 0.95 GeV.

$N_{up}(\mu)/N_{down}(\mu)$

VALUE	DOCUMENT ID	TECN	COMMENT
• • • We do not use the following data for averages, fits, limits, etc. • • •			
$0.551^{+0.035}_{-0.033}\pm0.004$	[26] ASHIE 05	SKAM	multi-GeV

[26] ASHIE 05 results are based on an exposure of 92 kton yr during the complete Super-Kamiokande I running period. The analyzed data sample consists of fully-contained single-ring μ-like events with visible energy > 1.33 GeV and partially-contained events. All partially-contained events are classified as μ-like. Upward-going events are those with $-1 <$ cos(zenith angle) < -0.2 and downward-going events are those with $0.2 <$ cos(zenith angle) <1. The μ-like up-down ratio for the multi-GeV data deviates from 1 (the expectation for no atmospheric ν_μ oscillations) by more than 12 standard deviations.

$N_{up}(e)/N_{down}(e)$

VALUE	DOCUMENT ID	TECN	COMMENT
• • • We do not use the following data for averages, fits, limits, etc. • • •			
$0.961^{+0.086}_{-0.079}\pm0.016$	[27] ASHIE 05	SKAM	multi-GeV

[27] ASHIE 05 results are based on an exposure of 92 kton yr during the complete Super-Kamiokande I running period. The analyzed data sample consists of fully-contained single-ring e-like events with visible energy > 1.33 GeV. Upward-going events are those with $-1 <$ cos(zenith angle) < -0.2 and downward-going events are those with $0.2 <$ cos(zenith angle) < 1. The e-like up-down ratio for the multi-GeV data is consistent with 1 (the expectation for no atmospheric ν_e oscillations).

Solar neutrinos

Solar neutrinos are produced by thermonuclear fusion reactions in the Sun. Radiochemical experiments measure particular combinations of fluxes from various neutrino-producing reactions, whereas water-Cherenkov experiments mainly measure a flux of neutrinos from decay of ^{8}B. Solar neutrino fluxes are composed of all active neutrino species, ν_e, ν_μ, and ν_τ. In addition, some other mechanisms may cause antineutrino components in solar neutrino fluxes. Each measurement method is sensitive to a particular component or a combination of components of solar neutrino fluxes. For details, see the following minireview.

SOLAR NEUTRINOS REVIEW

Revised September 2005 by K. Nakamura (KEK, High Energy Accelerator Research Organization, Japan).

1. Introduction

The Sun is a main-sequence star at a stage of stable hydrogen burning. It produces an intense flux of electron neutrinos

as a consequence of nuclear fusion reactions whose combined effect is

$$4p \rightarrow {}^4\mathrm{He} \ + 2e^+ + 2\nu_e. \qquad (1)$$

Positrons annihilate with electrons. Therefore, when considering the solar thermal energy generation, a relevant expression is

$$4p + 2e^- \rightarrow {}^4\mathrm{He} \ + 2\nu_e + 26.73 \text{ MeV} - E_\nu \ , \qquad (2)$$

where E_ν represents the energy taken away by neutrinos, with an average value being $\langle E_\nu \rangle \sim 0.6$ MeV. The neutrino-producing reactions which are at work inside the Sun are enumerated in the first column in Table 1. The second column in Table 1 shows abbreviation of these reactions. The energy spectrum of each reaction is shown in Fig. 1.

Observation of solar neutrinos directly addresses the theory of stellar structure and evolution, which is the basis of the standard solar model (SSM). The Sun as a well-defined neutrino source also provides extremely important opportunities to investigate nontrivial neutrino properties such as nonzero mass and mixing, because of the wide range of matter density and the great distance from the Sun to the Earth.

A pioneering solar neutrino experiment by Davis and collaborators using ^{37}Cl started in the late 1960's. From the very beginning of the solar-neutrino observation [1], it was recognized that the observed flux was significantly smaller than the SSM prediction, provided nothing happens to the electron neutrinos after they are created in the solar interior. This deficit has been called "the solar-neutrino problem."

In spite of the challenges by the chlorine and gallium radiochemical experiments (GALLEX, SAGE, and GNO) and water-Cherenkov experiments (Kamiokande and Super-Kamiokande), the solar-neutrino problem had persisted for more than 30 years.

However, there have been remarkable developments in the past five years and now the solar-neutrino problem has been finally solved.

In 2001, the initial result from SNO (Sudbury Neutrino Observatory) [2], a water Cherenkov detector with heavy water, on the solar-neutrino flux measured via charged-current (CC) reaction, $\nu_e d \to e^- pp$, combined with the Super-Kamiokande's high-statistics flux measurement via νe elastic scattering [3], provided direct evidence for flavor conversion of solar neutrinos [2]. Later in 2002, SNO's measurement of the neutral-current (NC) rate, $\nu d \to \nu pn$, and the updated CC result further strengthened this conclusion [4].

The most probable explanation which can also solve the solar-neutrino problem is neutrino oscillation. At this stage, the LMA (large mixing angle) solution was the most promising. However, at 3σ confidence level (CL), LOW (low probability or low mass) and/or VAC (vacuum) solutions were allowed depending on the method of analysis [5]. LMA and LOW are solutions of neutrino oscillation in matter [6,7] and VAC is a solution of neutrino oscillation in vacuum. Typical parameter values [5] corresponding to these solutions are

- LMA: $\Delta m^2 = 5.0 \times 10^{-5}$ eV^2, $\tan^2\theta = 0.42$
- LOW: $\Delta m^2 = 7.9 \times 10^{-8}$ eV^2, $\tan^2\theta = 0.61$
- VAC: $\Delta m^2 = 4.6 \times 10^{-10}$ eV^2, $\tan^2\theta = 1.8$.

It should be noted that all these solutions have large mixing angles. SMA (small mixing angle) solution (typical parameter values [5] are $\Delta m^2 = 5.0 \times 10^{-6}$ eV^2 and $\tan^2\theta = 1.5 \times 10^{-3}$) was once favored, but after SNO it was excluded at $> 3\sigma$ [5].

In December 2002, KamLAND (Kamioka Liquid Scintillator Anti-Neutrino Detector), a terrestrial $\bar{\nu}_e$ disappearance experiment using reactor neutrinos, observed clear evidence of

neutrino oscillation with the allowed parameter region overlapping with the parameter region of the LMA solution [8]. Assuming CPT invariance, this result directly implies that the true solution of the solar ν_e oscillation has been determined to be LMA. A combined analysis of all the solar-neutrino data and KamLAND data significantly constrained the allowed parameter region. Inside the LMA region, the allowed region splits into two bands with lower Δm^2 ($\sim 7 \times 10^{-5}$ eV^2, called LMA I) and higher Δm^2 ($\sim 2 \times 10^{-4}$ eV^2, called LMA II).

In September, 2003, SNO reported [9] salt-phase results on solar-neutrino fluxes observed with NaCl added in heavy water: this improved the sensitivity for the detection of the NC reaction. A global analysis of all the solar neutrino data combined with the KamLAND data restricted the allowed parameter region to the LMA I region at greater than 99% CL.

Recently, further results from KamLAND [10] significantly more constrained the allowed Δm^2 region. SNO also reported results from the complete salt phase [11]. A combined two-neutrino oscillation analysis [11] using the data from all solar-neutrino experiments and from KamLAND yields $\Delta m^2 = (8.0^{+0.6}_{-0.4}) \times 10^{-5}$ eV^2 and $\tan^2\theta = 0.45^{+0.09}_{-0.07}$ ($\theta = 33.9^{+2.4}_{-2.2}$ degrees).

2. Solar Model Predictions

A standard solar model is based on the standard theory of stellar evolution. A variety of input information is needed in the evolutionary calculations. The most elaborate SSM calculations have been developped by Bahcall and his collaborators, who define their SSM as the solar model which is constructed with the best available physics and input data. Though they used no helioseismological constraints in defining the SSM, favorable models show an excellent agreement between the calculated and

the helioseismologically-determined sound speeds to a precision of 0.1% rms throughout essentially the entire Sun. This greatly strengthens the confidence in the solar model. The currently preferred SSM is BS05(OP) developped by Bahcall and Serenelli [12,13]. This model uses newly calculated radiative opacities from the Opacity Project (OP) and previously standard heavy-element abundances (instead of the recently determined lower heavy-element abundances). The BS05(OP) prediction [12] for the fluxes from neutrino-producing reactions is given in Table 1. The solar-neutrino spectra calculated with this model [12], is shown in Fig. 1. The event rates in chlorine and gallium solar-neutrino experiments are calculated by scaling the BP2000 SSM results [14] (see Table 1 in p. 460 of 2004 edition of Review of Particle Physics [15]) to the BS05(OP) fluxes, and are shown in Table 2.

Other recent solar-model prediction for solar-neutrino fluxes is given by Turck-Chièze *et al.* [16]. Their model, called a seismic model [17], is based on the standard theory of stellar evolution where the best physics available is adopted, but some fundamental inputs such as the *pp* reaction rate and the heavy-element abundances in the Sun are seismically adjusted within the commonly estimated errors aiming at reducing the residual differences between the helioseismologically-determined and the model-calculated sound speeds. Their prediction for the event rates in chlorine and gallium solar-neutrino experiments as well as ^{8}B solar-neutrino flux is shown in the last line in Table 2.

Table 1: Neutrino-producing reactions in the Sun (first column) and their abbreviations (second column). The neutrino fluxes predicted by the BS05(OP) model [12] are listed in the third column. The theoretical errors of the neutrino fluxes are taken from "Historical (conservative)" errors given in Table 8 of Ref. [13].

Reaction	Abbr.	Flux ($\mathrm{cm}^{-2}\ \mathrm{s}^{-1}$)
$pp \to d\, e^+\, \nu$	*pp*	$5.99(1.00 \pm 0.01) \times 10^{10}$
$pe^-p \to d\, \nu$	*pep*	$1.42(1.00 \pm 0.02) \times 10^{8}$
$^3\mathrm{He}\ p \to {}^4\mathrm{He}\ e^+\nu$	*hep*	$7.93(1.00 \pm 0.16) \times 10^{3}$
$^7\mathrm{Be}\ e^- \to {}^7\mathrm{Li}\ \nu + (\gamma)$	^{7}Be	$4.84(1.00 \pm 0.11) \times 10^{9}$
$^8\mathrm{B} \to {}^8\mathrm{Be}^*\ e^+\nu$	^{8}B	$5.69(1.00 \pm 0.16) \times 10^{6}$
$^{13}\mathrm{N} \to {}^{13}\mathrm{C}\ e^+\nu$	^{13}N	$3.07(1.00^{+0.31}_{-0.28}) \times 10^{8}$
$^{15}\mathrm{O} \to {}^{15}\mathrm{N}\ e^+\nu$	^{15}O	$2.33(1.00^{+0.33}_{-0.29}) \times 10^{8}$
$^{17}\mathrm{F} \to {}^{17}\mathrm{O}\ e^+\nu$	^{17}F	$5.84(1.00 \pm 0.52) \times 10^{6}$

3. Solar Neutrino Experiments

So far, seven solar-neutrino experiments have published results. The most recent published results on the average event rates or flux from these experiments are listed in Table 2 and compared to the two recent solar-model predictions.

3.1. Radiochemical Experiments

Radiochemical experiments exploit electron neutrino absorption on nuclei followed by their decay through orbital electron capture. Produced Auger electrons are counted.

The Homestake chlorine experiment in USA uses the reaction

$$^{37}\mathrm{Cl} + \nu_e \to {}^{37}\mathrm{Ar} + e^- \ \text{(threshold 814 keV)}. \qquad (3)$$

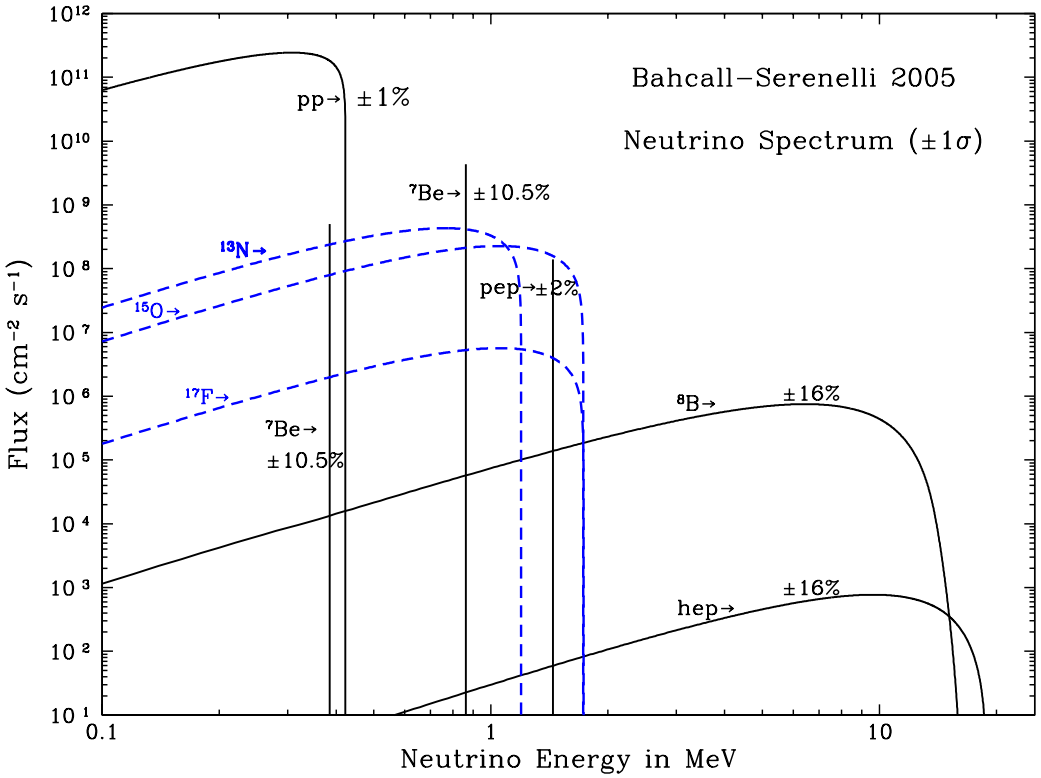

Figure 1: The solar neutrino spectrum predicted by the BS05(OP) standard solar model [12]. The neutrino fluxes from continuum sources are given in units of number $\mathrm{cm}^{-2}\mathrm{s}^{-1}\mathrm{MeV}^{-1}$ at one astronomical unit, and the line fluxes are given in number $\mathrm{cm}^{-2}\mathrm{s}^{-1}$. See full-color version on color pages at end of book.

Three gallium experiments (GALLEX and GNO at Gran Sasso in Italy and SAGE at Baksan in Russia) use the reaction

$$^{71}\mathrm{Ga} + \nu_e \rightarrow {}^{71}\mathrm{Ge} + e^- \ \text{(threshold 233 keV)}. \qquad (4)$$

The produced ^{37}Ar and ^{71}Ge atoms are both radioactive, with half lives ($\tau_{1/2}$) of 34.8 days and 11.43 days, respectively. After

Table 2: Results from the seven solar-neutrino experiments. Recent solar model calculations are also presented. The first and the second errors in the experimental results are the statistical and systematic errors, respectively. SNU (Solar Neutrino Unit) is defined as 10^{-36} neutrino captures per atom per second.

	$^{37}\mathrm{Cl}\rightarrow{}^{37}\mathrm{Ar}$ (SNU)	$^{71}\mathrm{Ga}\rightarrow{}^{71}\mathrm{Ge}$ (SNU)	$^{8}\mathrm{B}$ ν flux ($10^{6}\mathrm{cm}^{-2}\mathrm{s}^{-1}$)
Homestake			
(CLEVELAND 98)[18]	$2.56 \pm 0.16 \pm 0.16$	—	—
GALLEX			
(HAMPEL 99)[19]	—	$77.5 \pm 6.2^{+4.3}_{-4.7}$	—
GNO			
(ALTMANN 05)[20]	—	$62.9^{+5.5}_{-5.3} \pm 2.5$	—
GNO+GALLEX			
(ALTMANN 05)[20]	—	$69.3 \pm 4.1 \pm 3.6$	—
SAGE			
(ABDURASHI...02)[21]	—	$70.8^{+5.3+3.7}_{-5.2-3.2}$	—
Kamiokande			
(FUKUDA 96)[22]	—	—	$2.80 \pm 0.19 \pm 0.33^{\dagger}$
Super-Kamiokande			
(HOSAKA 05)[23]	—	—	$2.35 \pm 0.02 \pm 0.08^{\dagger}$
SNO (pure D_2O)			
(AHMAD 02)[4]	—	—	$1.76^{+0.06}_{-0.05} \pm 0.09^{\ddagger}$
	—	—	$2.39^{+0.24}_{-0.23} \pm 0.12^{\dagger}$
	—	—	$5.09^{+0.44+0.46*}_{-0.43-0.43}$
SNO (NaCl in D_2O)			
(AHARMIM 05)[11]	—	—	$1.68 \pm 0.06^{+0.08\ddagger}_{-0.09}$
	—	—	$2.35 \pm 0.22 \pm 0.15^{\dagger}$
	—	—	$4.94 \pm 0.21^{+0.38*}_{-0.34}$
BS05(OP) SSM [12]	8.1 ± 1.3	126 ± 10	$5.69(1.00 \pm 0.16)$
Seismic model [16]	7.64 ± 1.1	123.4 ± 8.2	5.31 ± 0.6

* Flux measured via the neutral-current reaction.

† Flux measured via νe elastic scattering.

‡ Flux measured via the charged-current reaction.

an exposure of the detector for two to three times $\tau_{1/2}$, the reaction products are chemically extracted and introduced into a low-background proportional counter, where they are counted for a sufficiently long period to determine the exponentially decaying signal and a constant background.

Solar-model calculations predict that the dominant contribution in the chlorine experiment comes from ^{8}B neutrinos, but ^{7}Be, *pep*, ^{13}N, and ^{15}O neutrinos also contribute. At present, the most abundant *pp* neutrinos can be detected only in gallium experiments. Even so, according to the solar-model calculations, almost half of the capture rate in the gallium experiments is due to other solar neutrinos.

The Homestake chlorine experiment was the first to attempt the observation of solar neutrinos. Initial results obtained in 1968 showed no events above background with upper limit for the solar-neutrino flux of 3 SNU [1]. After introduction of an improved electronics system which discriminates signal from background by measuring the rise time of the pulses from proportional counters, a finite solar-neutrino flux has been observed since 1970. The solar-neutrino capture rate shown in Table 2 is a combined result of 108 runs between 1970 and 1994 [18]. It is only about 1/3 of the solar-model predictions [12, 16].

GALLEX presented the first evidence of *pp* solar-neutrino observation in 1992 [24]. Here also, the observed capture rate is significantly less than the SSM prediction. SAGE initially reported very low capture rate, $20^{+15}_{-20} \pm 32$ SNU, with a 90% confidence-level upper limit of 79 SNU [25]. Later, SAGE [26] observed similar capture rate to that of GALLEX. Both GALLEX and SAGE groups tested the overall detector response with intense man-made ^{51}Cr neutrino sources, and observed good agreement between the measured ^{71}Ge production

rate and that predicted from the source activity, demonstrating the reliability of these experiments. The GALLEX Collaboration formally finished observations in early 1997. Since April, 1998, a newly defined collaboration, GNO (Gallium Neutrino Observatory) continued the observations until April 2003. The complete GNO results are published in Ref. [20]. The GNO + GALLEX joint analysis results are also presented [20] (see Table 2).

3.2 Kamiokande and Super-Kamiokande

Kamiokande and Super-Kamiokande in Japan are real-time experiments utilizing νe scattering

$$\nu_x + e^- \rightarrow \nu_x + e^- \tag{5}$$

in a large water-Cherenkov detector. It should be noted that the reaction Eq. (5) is sensitive to all active neutrinos, $x = e$, μ, and τ. However, the sensitivity to ν_μ and ν_τ is much smaller than the sensitivity to ν_e, $\sigma(\nu_{\mu,\tau}e) \approx 0.16\,\sigma(\nu_e e)$. The solar-neutrino flux measured via νe scattering is deduced assuming no neutrino oscillations.

These experiments take advantage of the directional correlation between the incoming neutrino and the recoil electron. This feature greatly helps the clear separation of the solar-neutrino signal from the background. Due to the high thresholds (7 MeV in Kamiokande and 5 MeV at present in Super-Kamiokande) the experiments observe pure ^{8}B solar neutrinos because *hep* neutrinos contribute negligibly according to the SSM.

The Kamiokande-II Collaboration started observing ^{8}B solar neutrinos at the beginning of 1987. Because of the strong directional correlation of νe scattering, this result gave the first direct evidence that the Sun emits neutrinos [27] (no directional information is available in radiochemical solar-neutrino

experiments). The observed solar-neutrino flux was also significantly less than the SSM prediction. In addition, Kamiokande-II obtained the energy spectrum of recoil electrons and the fluxes separately measured in the daytime and nighttime. The Kamiokande-II experiment came to an end at the beginning of 1995.

Super-Kamiokande is a 50-kton second-generation solar-neutrino detector, which is characterized by a significantly larger counting rate than the first-generation experiments. This experiment started observation in April 1996. In November 2001, Super-Kamiokande suffered from an accident in which substantial number of photomultiplier tubes were lost. The detector was rebuilt within a year with about half of the original number of photomultiplier tubes. The experiment with the detector before the accident is called Super-Kamiokande-I, and that after the accident is called Super-Kamiokande-II. The complete Super-Kamiokande-I solar-neutrino results are reported in Ref. [23]. The solar-neutrino flux is measured as a function of zenith angle and recoil-electron energy. The average solar-neutrino flux is given in Table 2. The observed day-night asymmetry is $A_{\rm DN} = \dfrac{\rm Day - Night}{0.5({\rm Day + Night})} = -0.021 \pm 0.020^{+0.013}_{-0.012}$. No indication of spectral distortion is observed.

3.3 SNO

In 1999, a new real time solar-neutrino experiment, SNO, in Canada started observation. This experiment uses 1000 tons of ultra-pure heavy water (D_2O) contained in a spherical acrylic vessel, surrounded by an ultra-pure H_2O shield. SNO measures ^{8}B solar neutrinos via the reactions

$$\nu_e + d \rightarrow e^- + p + p \qquad (6)$$

and

$$\nu_x + d \rightarrow \nu_x + p + n, \tag{7}$$

as well as νe scattering, Eq. (5). The CC reaction, Eq. (6), is sensitive only to electron neutrinos, while the NC reaction, Eq. (7), is sensitive to all active neutrinos.

The Q-value of the CC reaction is -1.4 MeV and the electron energy is strongly correlated with the neutrino energy. Thus, the CC reaction provides an accurate measure of the shape of the ^{8}B solar-neutrino spectrum. The contributions from the CC reaction and νe scattering can be distinguished by using different cos $\theta_\odot$ distributions where $\theta_\odot$ is the angle of the electron momentum with respect to the direction from the Sun to the Earth. While the νe scattering events have a strong forward peak, CC events have an approximate angular distribution of $1 - 1/3 \cos\theta_\odot$.

The threshold of the NC reaction is 2.2 MeV. In the pure D_2O, the signal of the NC reaction is neutron capture in deuterium, producing a 6.25-MeV γ-ray. In this case, the capture efficiency is low and the deposited energy is close to the detection threshold of 5 MeV. In order to enhance both the capture efficiency and the total γ-ray energy (8.6 MeV), 2 tons of NaCl were added to the heavy water in the second phase of the experiment. In addition, discrete ^{3}He neutron counters were installed and the NC measurement with them are being made as the third phase of the SNO experiment.

In 2001, SNO published the initial results on the measurement of the ^{8}B solar-neutrino flux via CC reaction [2]. The electron energy spectrum and the $\cos\theta_\odot$ distribution were also measured. The spectral shape of the electron energy was consistent with the expectations for an undistorted ^{8}B solar-neutrino spectrum.

SNO also measured the ^{8}B solar-neutrino flux via νe scattering [2]. Though the latter result had poor statistics, it was consistent with the high-statistics Super-Kamiokande result. Thus, the SNO group compared their CC result with Super-Kamiokande's νe scattering result, and obtained evidence of an active non-ν_e component in the solar-neutrino flux [2], as further described in Sec. 3.5.

Later, in April, 2002, SNO reported the first result on the ^{8}B solar-neutrino flux measurement via NC reaction [4]. The total flux measured via NC reaction was consistent with the solar-model predictions (see Table 2). Also, the SNO's CC and νe scattering results were updated [4]. These results were consistent with the earlier results [2].

The SNO Collaboration made a global analysis (see Sect. 3.6) of the SNO's day and night energy spectra together with the data from other solar-neutrino experiments. The results strongly favored the LMA solution, with the LOW solution allowed at 99.5% CL [28]. (In most of the similar global analyses, the VAC solution was also allowed at $99.9 \sim 99.73\%$ CL [5]) .

In September, 2003, SNO has released the first results of solar-neutrino flux measurements with dissolved NaCl in the heavy water [9]. The complete salt phase results are also reported recently [11]. Using the salt phase results, the SNO Collaboration made a global solar-neutrino analysis and a global solar + KamLAND analysis. Implications of these analyses are described in Sect. 5.

SNO also studied the energy spectrum and day-night flux asymmetries for both pure D_2O [28] and salt phases [11]. The energy spectrum deduced from the CC reaction is consistent with the spectrum expected from an undistorted ^{8}B spectral shape. No significant day-night flux asymmetries are observed

within uncertainties. These observations are consistent with the best-fit LMA solution from the global solar + KamLAND analysis.

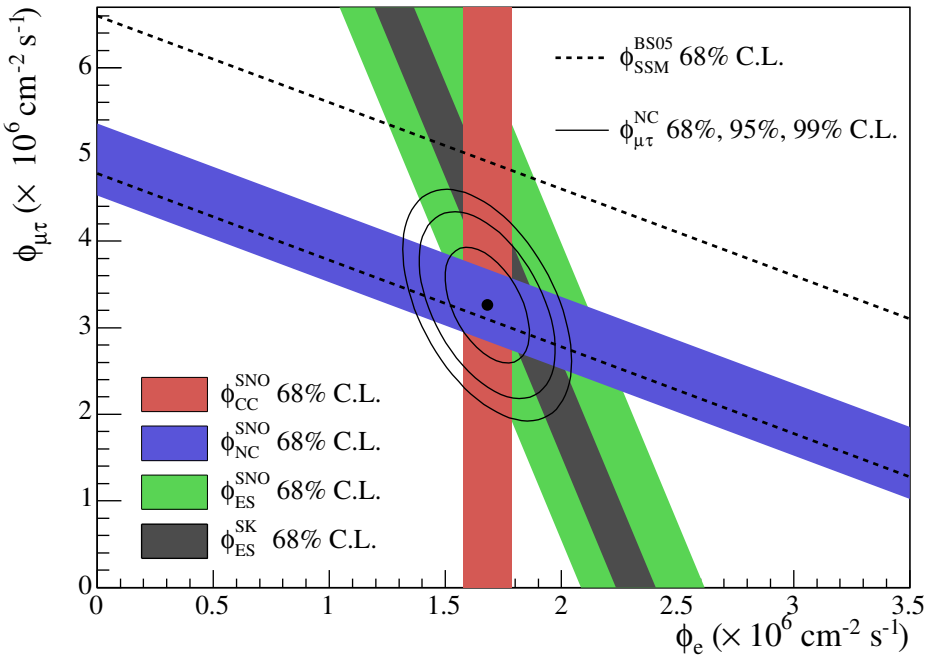

Figure 2: Fluxes of ^{8}B solar neutrinos, $\phi(\nu_e)$, and $\phi(\nu_{\mu \text{ or } \tau})$, deduced from the SNO's charged-current (CC), ν_e elastic scattering (ES), and neutral-current (NC) results for the salt phase measurement [11]. The Super-Kamiokande ES flux is from Ref. [34]. The BS05(OP) standard solar model prediction [12] is also shown. The bands represent the 1σ error. The contours show the 68%, 95%, and 99% joint probability for $\phi(\nu_e)$ and $\phi(\nu_{\mu \text{ or } \tau})$. This figure is taken from Ref. [11]. See full-color version on color pages at end of book.

3.4 Comparison of Experimental Results with Solar-Model Predictions

It is clearly seen from Table 2 that the results from all the solar-neutrino experiments, except the SNO's NC result, indicate significantly less flux than expected from the solar-model predictions [12, 16].

There has been a consensus that a consistent explanation of all the results of solar-neutrino observations is unlikely within the framework of astrophysics using the solar-neutrino spectra given by the standard electroweak model. Many authors made solar model-independent analyses constrained by the observed solar luminosity [29–33], where they attempted to fit the measured solar-neutrino capture rates and ^{8}B flux with normalization-free, undistorted energy spectra. All these attempts only obtained solutions with very low probabilities.

The data therefore suggest that the solution to the solar-neutrino problem requires nontrivial neutrino properties.

3.5 Evidence for Solar Neutrino Oscillations

Denoting the ^{8}B solar-neutrino flux obtained by the SNO's CC measurement as $\phi^{\rm CC}_{\rm SNO}(\nu_e)$ and that obtained by the Super-Kamiokande νe scattering as $\phi^{\rm ES}_{\rm SK}(\nu_x)$, $\phi^{\rm CC}_{\rm SNO}(\nu_e) = \phi^{\rm ES}_{\rm SK}(\nu_x)$ is expected for the standard neutrino physics. However, SNO's initial data [2] indicated

$$\phi^{\rm ES}_{\rm SK}(\nu_x) - \phi^{\rm CC}_{\rm SNO}(\nu_e) = (0.57 \pm 0.17) \times 10^6 \ \ {\rm cm}^{-2}{\rm s}^{-1}. \qquad (8)$$

The significance of the difference was $> 3\sigma$, implying direct evidence for the existence of a non-ν_e active neutrino flavor component in the solar-neutrino flux. A natural and most probable explanation of neutrino flavor conversion is neutrino oscillation. Note that both the SNO [2] and Super-Kamiokande [3] flux results were obtained by assuming the standard ^{8}B neutrino

spectrum shape. This assumption was justified by the measured energy spectra in both experiments.

The SNO's results for the pure D_2O phase, reported in 2002 [4], provided stronger evidence for neutrino oscillation than Eq. (8). The fluxes measured with CC, ES, and NC events were deduced. Here, the spectral distributions of the CC and ES events were constrained to an undistorted ^{8}B shape. The results are

$$\phi^{\rm CC}_{\rm SNO}(\nu_e) = (1.76^{+0.06}_{-0.05} \pm 0.09) \times 10^6 {\rm cm}^{-2}{\rm s}^{-1} \ , \qquad (9)$$

$$\phi^{\rm ES}_{\rm SNO}(\nu_x) = (2.39^{+0.24}_{-0.23} \pm 0.12) \times 10^6 {\rm cm}^{-2}{\rm s}^{-1} \ , \qquad (10)$$

$$\phi^{\rm NC}_{\rm SNO}(\nu_x) = (5.09^{+0.44+0.46}_{-0.43-0.43}) \times 10^6 {\rm cm}^{-2}{\rm s}^{-1} \ . \qquad (11)$$

Eq. (11) is a mixing-independent result and therefore tests solar models. It shows good agreement with the ^{8}B solar-neutrino flux predicted by the solar models [12, 16]. The flux of non-ν_e active neutrinos, $\phi(\nu_{\mu \text{ or } \tau})$, can be deduced from these results. It is

$$\phi(\nu_{\mu \text{ or } \tau}) = \left(3.41^{+0.66}_{-0.64}\right) \times 10^6 {\rm cm}^{-2}{\rm s}^{-1} \qquad (12)$$

where the statistical and systematic errors are added in quadrature. This $\phi(\nu_{\mu \text{ or } \tau})$ is 5.3 σ above 0. The non-zero $\phi(\nu_{\mu \text{ or } \tau})$ is strong evidence for neutrino flavor transformation.

From the salt phase measurement [11], the fluxes measured with CC and ES events were deduced with no constraint of the ^{8}B energy spectrum. The results are

$$\phi^{\rm CC}_{\rm SNO}(\nu_e) = (1.68 \pm 0.06^{+0.08}_{-0.09}) \times 10^6 {\rm cm}^{-2}{\rm s}^{-1} \ , \qquad (13)$$

$$\phi^{\rm ES}_{\rm SNO}(\nu_x) = (2.35 \pm 0.22 \pm 0.15) \times 10^6 {\rm cm}^{-2}{\rm s}^{-1} \ , \qquad (14)$$

$$\phi^{\rm NC}_{\rm SNO}(\nu_x) = (4.94 \pm 0.21^{+0.38}_{-0.34}) \times 10^6 {\rm cm}^{-2}{\rm s}^{-1} \ . \qquad (15)$$

These results are consistent with the results from the pure D_2O phase. Fig. 2 shows the salt phase result of $\phi(\nu_{\mu \text{ or } \tau})$ versus the flux of electron neutrinos $\phi(\nu_e)$ with the 68%, 95%, and 99% joint probability contours.

4. KamLAND Reactor Neutrino Oscillation Experiment

KamLAND is a 1-kton ultra-pure liquid scintillator detector located at the old Kamiokande's site in Japan. Although the ultimate goal of KamLAND is observation of ^{7}Be solar neutrinos with much lower energy threshold, the initial phase of the experiment is a long baseline (flux-weighted average distance of $\sim$ 180 km) neutrino oscillation experiment using $\bar{\nu}_e$'s emitted from power reactors. The reaction $\bar{\nu}_e + p \rightarrow e^+ + n$ is used to detect reactor $\bar{\nu}_e$'s and delayed coincidence with 2.2 MeV γ-ray from neutron capture on a proton is used to reduce the backgrounds.

With the reactor $\bar{\nu}_e$'s energy spectrum (< 8 MeV) and a prompt-energy analysis threshold of 2.6 MeV, this experiment has a sensitive Δm^2 range down to $\sim 10^{-5}$ eV^2. Therefore, if the LMA solution is the real solution of the solar neutrino problem, KamLAND should observe reactor $\bar{\nu}_e$ disappearance, assuming CPT invariance.

The first KamLAND results [8] with 162 ton·yr exposure were reported in December 2002. The ratio of observed to expected (assuming no neutrino oscillation) number of events was

$$\frac{N_{\text{obs}} - N_{\text{BG}}}{N_{\text{NoOsc}}} = 0.611 \pm 0.085 \pm 0.041. \qquad (16)$$

with obvious notation. This result shows clear evidence of event deficit expected from neutrino oscillation. The 95% CL allowed regions are obtained from the oscillation analysis with the observed event rates and positron spectrum shape. There are

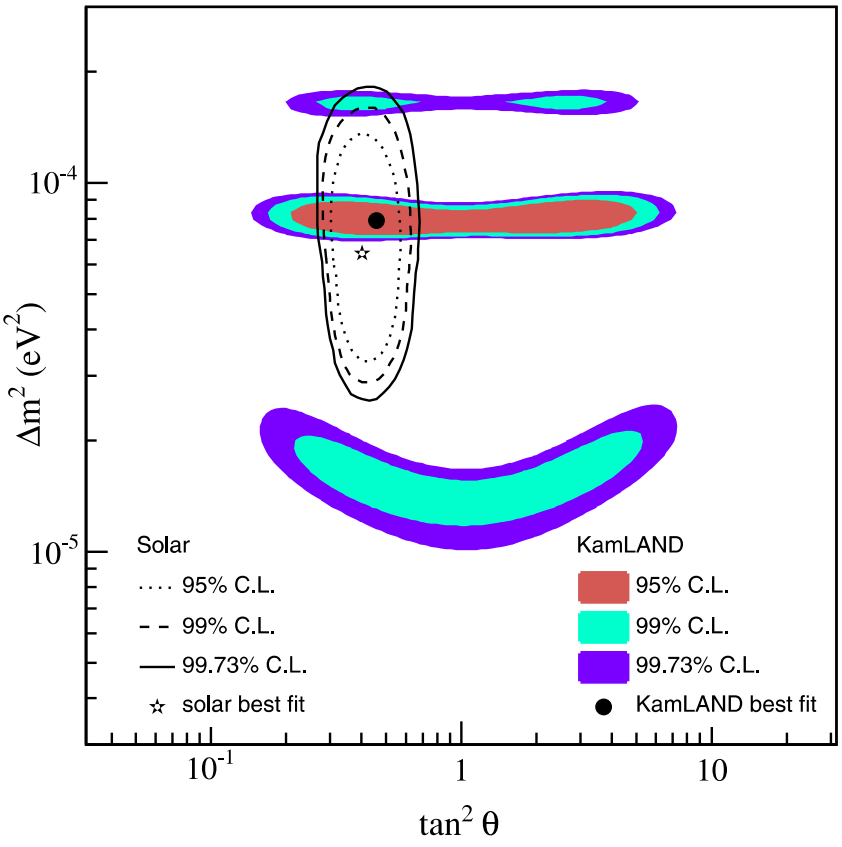

Figure 3: Allowed regions of neutrino-oscillation parameters from the KamLAND 766 ton·yr exposure $\bar{\nu}_e$ data [10]. The LMA region from solar-neutrino experiments [9] is also shown. This figure is taken from Ref. [10]. See full-color version on color pages at end of book.

two bands of regions allowed by both solar and KamLAND data in the region. The LOW and VAC solutions are excluded by the KamLAND results. A combined global solar + KamLAND analysis showed that the LMA is a unique solution to the solar neutrino problem with $> 5\sigma$ CL [35].

In June 2004, KamLAND released the results from 766 ton·yr exposure [10]. In addition to the deficit of events, the observed positron spectrum showed the distortion expected from neutrino oscillation. Fig. 3 shows the allowed regions in the neutrino-oscillation parameter space. The best-fit point lies in the region called LMA I. The LMA II region is disfavored at the 98% CL.

5. Global Neutrino Oscillation Analysis

The SNO Collaboration updated [11] a global two-neutrino oscillation analysis of the solar-neutrino data including the SNO's complete salt phase data, and global solar + KamLAND 766 ton·yr data [10]. The resulting neutrino oscillation contours are shown in Fig. 4. The best fit parameters for the global solar analysis are $\Delta m^2 = 6.5^{+4.4}_{-2.3} \times 10^{-5}$ eV^2 and $\tan^2\theta = 0.45^{+0.09}_{-0.08}$. The inclusion of the KamLAND data significantly constrains the allowed Δm^2 region, but shifts the best-fit Δm^2 value. The best-fit parameters for the global solar + KamLAND analysis are $\Delta m^2 = 8.0^{+0.6}_{-0.4} \times 10^{-5}$ eV^2 and $\tan^2\theta = 0.45^{+0.09}_{-0.07}$ ($\theta = 33.9^{+2.4}_{-2.2}$).

A number of authors [36 - 38] also made combined global neutrino oscillation analysis of solar + KamLAND data in mostly three-neutrino oscillation framework using the SNO complete salt phase data [11] and the KamLAND 766 ton·yr data [10]. These give consistent results with the SNO's two-neutrino oscillation analysis [11].

6. Future Prospects

Now that the solar-neutrino problem has been essentially solved, what are the future prospects of the solar-neutrino experiments?

From the particle-physics point of view, precise determination of the oscillation parameters and search for non-standard physics such as a small admixture of a sterile component in the solar-neutrino flux will be still of interest. More precise NC measurements by SNO will contribute in reducing the uncertainty of the mixing angle [39]. Measurements of the pp flux to an accuracy comparable to the quoted accuracy ($\pm 1\%$) of the SSM calculation will significantly improve the precision of the mixing angle [40,41].

An important task of the future solar neutrino experiments is further tests of the SSM by measuring monochromatic ^{7}Be neutrinos and fundamental *pp* neutrinos. The ^{7}Be neutrino flux will be measured by a new experiment, Borexino, at Gran Sasso via νe scattering in 300 tons of ultra-pure liquid scintillator with a detection threshold as low as 250 keV. KamLAND will also observe ^{7}Be neutrinos if the detection threshold can be lowered to a level similar to that of Borexino.

For the detection of *pp* neutrinos, various ideas for the detection scheme have been presented. However, no experiments have been approved yet, and extensive R&D efforts are still needed for any of these ideas to prove its feasibility.

References

1. D. Davis, Jr., D.S. Harmer, and K.C. Hoffman, Phys. Rev. Lett. **20**, 1205 (1968).
2. Q.R. Ahmad *et al.*, Phys. Rev. Lett. **87**, 071301 (2001).
3. Y. Fukuda *et al.*, Phys. Rev. Lett. **86**, 5651 (2001).
4. Q.R. Ahmad *et al.*, Phys. Rev. Lett. **89**, 011301 (2002).

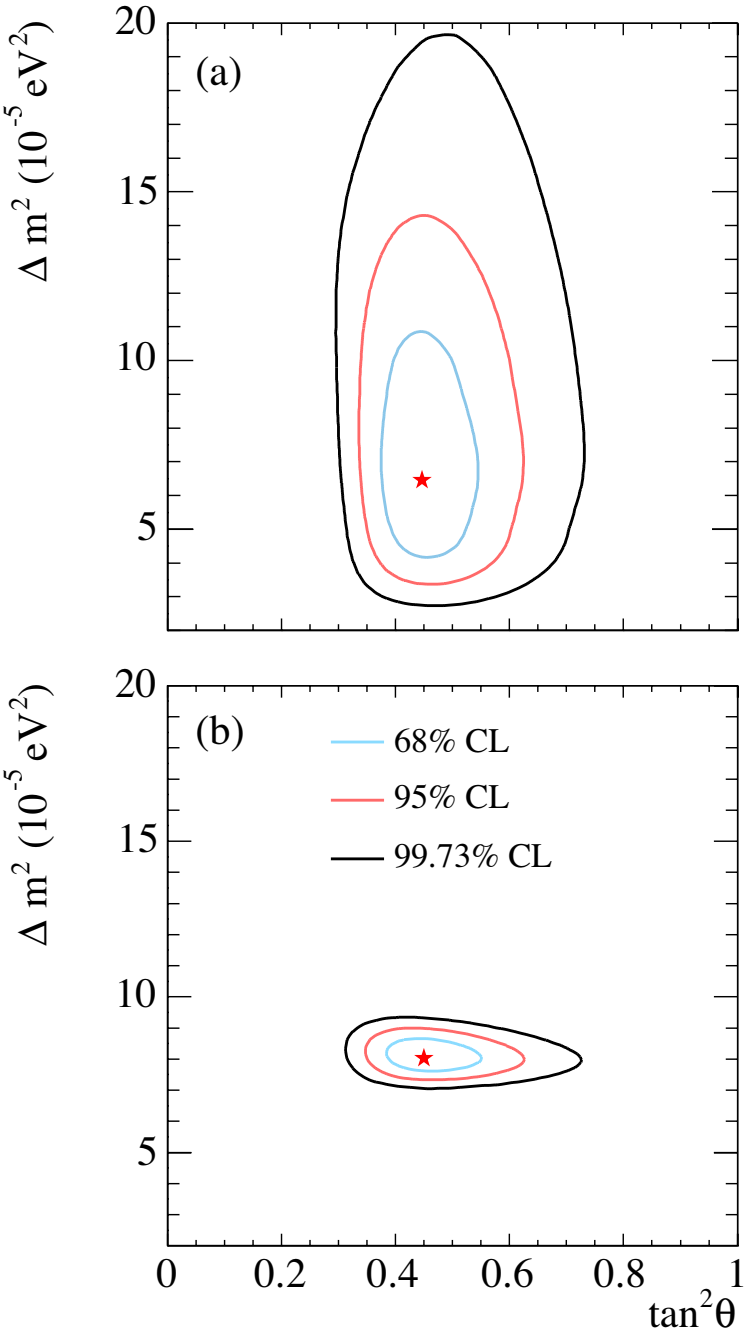

Figure 4: Update of the global neutrino oscillation contours given by the SNO Collaboration assuming that the ^{8}B neutrino flux is free and the *hep* neutrino flux is fixed. (a) Solar global analysis. (b) Solar global + KamLAND. This figure is taken from Ref. [11]. See full-color version on color pages at end of book.

5. See, for example, J.N. Bahcall, C.M. Gonzalez-Garcia, and C. Peña-Garay, JHEP 0207, 054 (2002).
6. L. Wolfenstein, Phys. Rev. **D17**, 2369 (1978).
7. S.P. Mikheyev and A. Yu. Smirnov, Sov. J. Nucl. Phys. **42**, 913 (1985).
8. K. Eguchi *et al.*, Phys. Rev. Lett. **90**, 021802 (2003).
9. S.N. Ahmed *et al.*, Phys. Rev. Lett. **92**, 181301 (2004).
10. T. Araki *et al.*, Phys. Rev. Lett. **94**, 081801 (2005).
11. B. Aharmim *et al.*, `nucl-ex/0502021`.
12. J.N. Bahcall, A.M. Serenelli, and S. Basu, Astrophys. J. **621**, L85 (2005).
13. J.N. Bahcall and A.M. Serenelli Astrophys. J. **626**, 530 (2005).
14. J.N. Bahcall, M.H. Pinsonneault, and S. Basu, Astrophys. J. **555**, 990 (2001).
15. S. Eidelman *et al.*, Phys. Lett. **B592**, 1 (2004).
16. S. Turck-Chièze *et al.*, Phys. Rev. Lett. **93**, 211102 (2004).
17. S. Couvidat, S. Turck-Chièze, and A.G. Kosovichev, Astrophys. J. **599**, 1434 (2003).
18. B.T. Cleveland *et al.*, Ap. J. **496**, 505 (1998).
19. W. Hampel *et al.*, Phys. Lett. **B447**, 127 (1999).
20. M. Altmann *et al.*, Phys. Lett. **B616**, 174 (2005).
21. J.N. Abdurashitov *et al.*, Sov. Phys. JETP **95**, 181 (2002).
22. Y. Fukuda *et al.*, Phys. Rev. Lett. **77**, 1683 (1996).
23. J. Hosaka *et al.*, `hep-ex/0508053`.
24. P. Anselmann *et al.*, Phys. Lett. **B285**, 376 (1992).
25. A.I. Abazov *et al.*, Phys. Rev. Lett. **67**, 3332 (1991).
26. J.N. Abdurashitov *et al.*, Phys. Lett. **B328**, 234 (1994).
27. K.S. Hirata *et al.*, Phys. Rev. Lett. **63**, 16 (1989).
28. Q.R. Ahmad *et al.*, Phys. Rev. Lett. **89**, 011302 (2002).
29. N. Hata, S. Bludman, and P. Langacker, Phys. Rev. **D49**, 3622 (1994).
30. N. Hata and P. Langacker, Phys. Rev. **D52**, 420 (1995).

31. N. Hata and P. Langacker, Phys. Rev. **D56**, 6107 (1997).
32. S. Parke, Phys. Rev. Lett. **74**, 839 (1995).
33. K.M. Heeger and R.G.H. Robertson, Phys. Rev. Lett. **77**, 3720 (1996).
34. Y. Fukuda *et al.*, Phys. Lett. **B539**, 179 (2002).
35. See, for example, J.N. Bahcall, M.C. Gonzalez-Garcia, and C. Peña-Garay, JHEP 0302, 009 (2003).
36. A.B. Balantekin *et al.*, Phys. Lett. **B613**, 61 (2005).
37. A. Strumia and F. Vissani, `hep-ph/0503246`.
38. G.L. Fogli *et al.*, `hep-ph/0506083`.
39. A. Bandyopadhyay *et al.*, Phys. Lett. **B608**, 115 (2005).
40. J.N. Bahcall and C. Peña-Garay, JHEP 0311, 004 (2003).
41. A. Bandyopadhyay *et al.*, Phys. Rev. **D72**, 033013 (2005).

ν_e Capture Rates from Radiochemical Experiments

1 SNU (Solar Neutrino Unit) = 10^{-36} captures per atom per second.

VALUE (SNU)	*DOCUMENT ID*		*TECN*	*COMMENT*
• • • We do not use the following data for averages, fits, limits, etc. • • •				
$62.9\ ^{+5.5}_{-5.3}\ \pm2.5$	[28] ALTMANN	05	GNO	^{71}Ga → ^{71}Ge
$69.3\ \pm4.1\ \pm3.6$	[29] ALTMANN	05	GNO	GNO + GALX combined
$70.8\ ^{+5.3}_{-5.2}\ ^{+3.7}_{-3.2}$	[30] ABDURASHI...	02	SAGE	^{71}Ga → ^{71}Ge
$77.5\ \pm6.2\ ^{+4.3}_{-4.7}$	[31] HAMPEL	99	GALX	^{71}Ga → ^{71}Ge
$2.56\pm0.16\pm0.16$	[32] CLEVELAND	98	HOME	^{37}Cl → ^{37}Ar

[28] ALTMANN 05 reports the complete result from the GNO solar neutrino experiment (GNO I+II+III), which is the successor project of GALLEX. Experimental technique of GNO is essentially the same as that of GALLEX. The run data cover the period 20 May 1998 through 9 April 2003.

[29] Combined result of GALLEX I+II+III+IV (HAMPEL 99) and GNO I+II+III.

[30] ABDURASHITOV 02 report a combined analysis of 92 runs of the SAGE solar-neutrino experiment during the period January 1990 through December 2001, and updates the ABDURASHITOV 99B result. A total of 406.4 ^{71}Ge events were observed. No evidence was found for temporal variations of the neutrino capture rate over the entire observation period.

[31] HAMPEL 99 report the combined result for GALLEX I+II+III+IV (65 runs in total), which update the HAMPEL 96 result. The GALLEX IV result (12 runs) is $118.4 \pm 17.8 \pm 6.6$ SNU. (HAMPEL 99 discuss the consistency of partial results with the mean.) The GALLEX experimental program has been completed with these runs. The total run data cover the period 14 May 1991 through 23 January 1997. A total of 300 ^{71}Ge events were observed.

[32] CLEVELAND 98 is a detailed report of the ^{37}Cl experiment at the Homestake Mine. The average solar neutrino-induced ^{37}Ar production rate from 108 runs between 1970 and 1994 updates the DAVIS 89 result.

ϕ_{ES} (^{8}B)

^{8}B solar-neutrino flux measured via νe elastic scattering. This process is sensitive to all active neutrino flavors, but with reduced sensitivity to ν_μ, ν_τ due to the cross-section difference, $\sigma(\nu_{\mu,\tau} e) \sim 0.16\sigma(\nu_e e)$. If the ^{8}B solar-neutrino flux involves nonelectron flavor active neutrinos, their contribution to the flux is ~ 0.16 times of ν_e.

VALUE (10^6 cm^{-2}s^{-1})	*DOCUMENT ID*		*TECN*	*COMMENT*
• • • We do not use the following data for averages, fits, limits, etc. • • •				
$2.35 \pm 0.22 \pm 0.15$	[33] AHARMIM	05A	SNO	Salty D_2O; ^{8}B shape not constrained
$2.34 \pm 0.23^{+0.15}_{-0.14}$	[33] AHARMIM	05A	SNO	Salty D_2O; ^{8}B shape constrained
$2.39^{+0.24}_{-0.23} \pm 0.12$	[34] AHMAD	02	SNO	average flux
$2.35 \pm 0.03^{+0.07}_{-0.06}$	[35] FUKUDA	02	SKAM	average flux
$2.39 \pm 0.34^{+0.16}_{-0.14}$	[36] AHMAD	01	SNO	average flux
$2.80 \pm 0.19 \pm 0.33$	[37] FUKUDA	96	KAMI	average flux
2.70 ± 0.27	[37] FUKUDA	96	KAMI	day flux
$2.87^{+0.27}_{-0.26}$	[37] FUKUDA	96	KAMI	night flux

[33] AHARMIM 05A measurements were made with dissolved NaCl (0.195% by weight) in heavy water over the period between July 26, 2001 and August 28, 2003, corresponding to 391.4 live days, and update AHMED 04A. The *CC*, *ES*, and *NC* events were statistically separated. In one method, the ^{8}B energy spectrum was not constrained. In the other method, the constraint of an undistorted ^{8}B energy spectrum was added for comparison with AHMAD 02 results.

[34] AHMAD 02 reports the ^{8}B solar-neutrino flux measured via νe elastic scattering above the kinetic energy threshold of 5 MeV. The data correspond to 306.4 live days with SNO between November 2, 1999 and May 28, 2001, and updates AHMAD 01 results.

[35] FUKUDA 02 results are for 1496 live days with Super-Kamiokande between May 31, 1996 and July 15, 2001, and replace FUKUDA 01 results. The analysis threshold is 5 MeV except for the first 280 live days (6.5 MeV).

[36] AHMAD 01 reports the ^{8}B solar-neutrino flux measured via νe elastic scattering above the kinetic energy threshold of 6.75 MeV. The data correspond to 241 live days with SNO between November 2, 1999 and January 15, 2001.

[37] FUKUDA 96 results are for a total of 2079 live days with Kamiokande II and III from January 1987 through February 1995, covering the entire solar cycle 22, with threshold $E_e > 9.3$ MeV (first 449 days), > 7.5 MeV (middle 794 days), and > 7.0 MeV (last 836 days). These results update the HIRATA 90 result for the average ^{8}B solar-neutrino flux and HIRATA 91 result for the day-night variation in the ^{8}B solar-neutrino flux. The total data sample was also analyzed for short-term variations: within experimental errors, no strong correlation of the solar-neutrino flux with the sunspot numbers was found.

ϕ_{CC} (^{8}B)

^{8}B solar-neutrino flux measured with charged-current reaction which is sensitive exclusively to ν_e.

VALUE (10^6 cm^{-2}s^{-1})	*DOCUMENT ID*		*TECN*	*COMMENT*
• • • We do not use the following data for averages, fits, limits, etc. • • •				
$1.68 \pm 0.06^{+0.08}_{-0.09}$	[38] AHARMIM	05A	SNO	Salty D_2O; ^{8}B shape not const.

$1.72 \pm 0.05 \pm 0.11$	[38] AHARMIM	05A	SNO	Salty D_2O; ^8B shape constrained
$1.76^{+0.06}_{-0.05} \pm 0.09$	[39] AHMAD	02	SNO	average flux
$1.75 \pm 0.07^{+0.12}_{-0.11} \pm 0.05$	[40] AHMAD	01	SNO	average flux

[38] AHARMIM 05A measurements were made with dissolved NaCl (0.195% by weight) in heavy water over the period between July 26, 2001 and August 28, 2003, corresponding to 391.4 live days, and update AHMED 04A. The *CC*, *ES*, and *NC* events were statistically separated. In one method, the ^8B energy spectrum was not constrained. In the other method, the constraint of an undistorted ^8B energy spectrum was added for comparison with AHMAD 02 results.

[39] AHMAD 02 reports the SNO result of the ^8B solar-neutrino flux measured with charged-current reaction on deuterium, $\nu_e d \rightarrow pp e^-$, above the kinetic energy threshold of 5 MeV. The data correspond to 306.4 live days with SNO between November 2, 1999 and May 28, 2001, and updates AHMAD 01 results.

[40] AHMAD 01 reports the first SNO result of the ^8B solar-neutrino flux measured with the charged-current reaction on deuterium, $\nu_e d \rightarrow pp e^-$, above the kinetic energy threshold of 6.75 MeV. The data correspond to 241 live days with SNO between November 2, 1999 and January 15, 2001.

ϕ_{NC} (^8B)

^8B solar neutrino flux measured with neutral-current reaction, which is equally sensitive to ν_e, ν_μ, and ν_τ.

VALUE (10^6 cm^{-2}s^{-1})	*DOCUMENT ID*	*TECN*	*COMMENT*
• • • We do not use the following data for averages, fits, limits, etc. • • •			
$4.94 \pm 0.21^{+0.38}_{-0.34}$	[41] AHARMIM	05A	SNO Salty D_2O; ^8B shape not const.
$4.81 \pm 0.19^{+0.28}_{-0.27}$	[41] AHARMIM	05A	SNO Salty D_2O; ^8B shape constrained
$5.09^{+0.44}_{-0.43}{}^{+0.46}_{-0.43}$	[42] AHMAD	02	SNO average flux; ^8B shape const.
$6.42 \pm 1.57^{+0.55}_{-0.58}$	[42] AHMAD	02	SNO average flux; ^8B shape not const.

[41] AHARMIM 05A measurements were made with dissolved NaCl (0.195% by weight) in heavy water over the period between July 26, 2001 and August 28, 2003, corresponding to 391.4 live days, and update AHMED 04A. The *CC*, *ES*, and *NC* events were statistically separated. In one method, the ^8B energy spectrum was not constrained. In the other method, the constraint of an undistorted ^8B energy spectrum was added for comparison with AHMAD 02 results.

[42] AHMAD 02 reports the first SNO result of the ^8B solar-neutrino flux measured with the neutral-current reaction on deuterium, $\nu_\ell d \rightarrow np\nu_\ell$, above the neutral-current reaction threshold of 2.2 MeV. The data correspond to 306.4 live days with SNO between November 2, 1999 and May 28, 2001.

$\phi_{\nu_\mu+\nu_\tau}$ (^8B)

Nonelectron-flavor active neutrino component (ν_μ and ν_τ) in the ^8B solar-neutrino flux.

VALUE (10^6 cm^{-2}s^{-1})	*DOCUMENT ID*	*TECN*	*COMMENT*
• • • We do not use the following data for averages, fits, limits, etc. • • •			

$3.26 \pm 0.25^{+0.40}_{-0.35}$	[43] AHARMIM	05A	SNO	From ϕ_{NC}, ϕ_{CC}, and ϕ_{ES}; ^{8}B shape not const.
$3.09 \pm 0.22^{+0.30}_{-0.27}$	[43] AHARMIM	05A	SNO	From ϕ_{NC}, ϕ_{CC}, and ϕ_{ES}; ^{8}B shape constrained
$3.41 \pm 0.45^{+0.48}_{-0.45}$	[44] AHMAD	02	SNO	From ϕ_{NC}, ϕ_{CC}, and ϕ_{ES}
3.69 ± 1.13	[45] AHMAD	01		Derived from SNO+SuperKam, water Cherenkov

[43] AHARMIM 05A measurements were made with dissolved NaCl (0.195% by weight) in heavy water over the period between July 26, 2001 and August 28, 2003, corresponding to 391.4 live days, and update AHMED 04A. The *CC*, *ES*, and *NC* events were statistically separated. In one method, the ^{8}B energy spectrum was not constrained. In the other method, the constraint of an undistorted ^{8}B energy spectrum was added for comparison with AHMAD 02 results.

[44] AHMAD 02 deduced the nonelectron-flavor active neutrino component (ν_μ and ν_τ) in the ^{8}B solar-neutrino flux, by combining the charged-current result, the νe elastic-scattering result and the neutral-current result.

[45] AHMAD 01 deduced the nonelectron-flavor active neutrino component (ν_μ and ν_τ) in the ^{8}B solar-neutrino flux, by combining the SNO charged-current result (AHMAD 01) and the Super-Kamiokande νe elastic-scattering result (FUKUDA 01).

Total Flux of Active ^{8}B Solar Neutrinos

Total flux of active neutrinos (ν_e, ν_μ, and ν_τ).

VALUE (10^6 cm^{-2}s^{-1})	*DOCUMENT ID*	*TECN*	*COMMENT*
• • • We do not use the following data for averages, fits, limits, etc. • • •			
$4.94 \pm 0.21^{+0.38}_{-0.34}$	[46] AHARMIM	05A	SNO From ϕ_{NC}; ^{8}B shape not const.
$4.81 \pm 0.19^{+0.28}_{-0.27}$	[46] AHARMIM	05A	SNO From ϕ_{NC}; ^{8}B shape constrained
$5.09^{+0.44}_{-0.43}{}^{+0.46}_{-0.43}$	[47] AHMAD	02	SNO Direct measurement from ϕ_{NC}
5.44 ± 0.99	[48] AHMAD	01	Derived from SNO+SuperKam, water Cherenkov

[46] AHARMIM 05A measurements were made with dissolved NaCl (0.195% by weight) in heavy water over the period between July 26, 2001 and August 28, 2003, corresponding to 391.4 live days, and update AHMED 04A. The *CC*, *ES*, and *NC* events were statistically separated. In one method, the ^{8}B energy spectrum was not constrained. In the other method, the constraint of an undistorted ^{8}B energy spectrum was added for comparison with AHMAD 02 results.

[47] AHMAD 02 determined the total flux of active ^{8}B solar neutrinos by directly measuring the neutral-current reaction, $\nu_\ell d \rightarrow np\nu_\ell$, which is equally sensitive to ν_e, ν_μ, and ν_τ.

[48] AHMAD 01 deduced the total flux of active ^{8}B solar neutrinos by combining the SNO charged-current result (AHMAD 01) and the Super-Kamiokande νe elastic-scattering result (FUKUDA 01).

Day-Night Asymmetry (^{8}B)

$A = (\phi_{\text{night}} - \phi_{\text{day}}) / \phi_{\text{average}}$

VALUE	DOCUMENT ID		TECN	COMMENT
• • • We do not use the following data for averages, fits, limits, etc. • • •				
$-0.056 \pm 0.074 \pm 0.053$	[49] AHARMIM	05A	SNO	From salty SNO ϕ_{CC}
$-0.037 \pm 0.063 \pm 0.032$	[49] AHARMIM	05A	SNO	From salty SNO ϕ_{CC}; const. of no ϕ_{NC} asymmetry
$0.018 \pm 0.016^{+0.013}_{-0.012}$	[50] SMY	04	SKAM	Fitted in the LMA region
$0.14 \pm 0.063^{+0.015}_{-0.014}$	[51] AHMAD	02B	SNO	Derived from SNO ϕ_{CC}
$0.07 \pm 0.049^{+0.013}_{-0.012}$	[52] AHMAD	02B	SNO	Const. of no ϕ_{NC} asymmetry
$0.021 \pm 0.020^{+0.013}_{-0.012}$	[53] FUKUDA	02	SKAM	Based on ϕ_{ES}

[49] AHARMIM 05A measurements were made with dissolved NaCl (0.195% by weight) in heavy water over the period between July 26, 2001 and August 28, 2003, with 176.5 days of the live time recorded during the day and 214.9 days during the night. This result is obtained with the spectral distribution of the CC events not constrained to the ^{8}B shape.

[50] SMY 04 obtained this result for the best-fit LMA oscillation parameters determined by fitting the time variation of the solar neutrino flux measured via ν_e elastic scattering to the variations expected from neutrino oscillations. The directly measured result is given by FUKUDA 02.

[51] AHMAD 02B results are based on the charged-current interactions recorded between November 2, 1999 and May 28, 2001, with the day and night live times of 128.5 and 177.9 days, respectively.

[52] AHMAD 02B results are derived from the charged-current interactions, neutral-current interactions, and νe elastic scattering, with the total flux of active neutrinos constrained to have no asymmetry. The data were recorded between November 2, 1999 and May 28, 2001, with the day and night live times of 128.5 and 177.9 days, respectively.

[53] FUKUDA 02 results are for 1496 live days with Super-Kamiokande between May 31, 1996 and July 15, 2001, and replace FUKUDA 01 results. The analysis threshold is 5 MeV except for the first 280 live days (6.5 MeV).

ϕ_{ES} (hep)

hep solar-neutrino flux measured via νe elastic scattering. This process is sensitive to all active neutrino flavors, but with reduced sensitivity to ν_μ, ν_τ due to the cross-section difference, $\sigma(\nu_{\mu,\tau} e) \sim 0.16\sigma(\nu_e e)$. If the hep solar-neutrino flux involves nonelectron flavor active neutrinos, their contribution to the flux is ~ 0.16 times of ν_e.

VALUE (10^3 cm^{-2}s^{-1})	CL%	DOCUMENT ID		TECN
<40	90	[54] FUKUDA	01	SKAM

[54] FUKUDA 01 result is obtained from the recoil electron energy window of 18–21 MeV, and the obtained 90% confidence level upper limit is 4.3 times the BP2000 Standard-Solar-Model prediction.

$\phi_{\overline{\nu}_e}$ (^{8}B)

Searches are made for electron antineutrino flux from the Sun. Flux limits listed here are derived relative to the BP2000 Standard Solar Model ^{8}B solar neutrino flux, with an assumption that solar $\overline{\nu}_e$s follow an unoscillated ^{8}B neutrino spectrum.

VALUE (%)	*CL%*	*DOCUMENT ID*		*TECN*	*COMMENT*
• • • We do not use the following data for averages, fits, limits, etc. • • •					
<0.81	90	AHARMIM	04	SNO	4.0< $E_{\overline{\nu}_e}$ < 14.8 MeV
<0.028	90	EGUCHI	04	KLND	8.3< $E_{\overline{\nu}_e}$ < 14.8 MeV
<0.8	90	GANDO	03	SKAM	8.0< $E_{\overline{\nu}_e}$ < 20.0 MeV

(B) Three-neutrino mixing parameters

INTRODUCTION TO THREE-NEUTRINO MIXING PARAMETERS LISTINGS

Written April 2006 by M. Goodman (ANL)

Introduction and Notation: With the exception of the LSND anomaly, current accelerator, reactor, solar and atmospheric neutrino data can be described within the framework of a 3×3 mixing matrix between the flavor eigenstates ν_e, ν_μ, and ν_τ and mass eigenstates ν_1, ν_2 and ν_3. (See Eq. (13.32) of the Review "Neutrino Mass, Mixing and Flavor Change" by B. Kayser.) Whether or not this is the ultimately correct framework, it is currently widely used to parametrize neutrino mixing data and to plan new experiments.

The mass differences are called Δm^2_{21} and Δm^2_{32} following Eq. (13.30) in the review. In these Listings, we assume that $\Delta m^2_{31} \sim \Delta m^2_{32}$, although in the future, experiments may be precise enough to measure these separately. The angles, as specified in Eq. (13.31) of the review, are labeled θ_{12}, θ_{23}, and θ_{13}. The *CP* violating phase is called δ, but that does not yet appear in the Listings. The familiar two neutrino form for oscillations is given in Eqs. (13.18) and (13.19). Despite the fact that the mixing angles have been measured to be much larger than in the quark sector, the two-neutrino form is often

a very good approximation and is used in many situations. This is possible thanks to the existence of two small numbers, $\Delta m^2_{21}/\Delta m^2_{32} \ll 1$, $\sin^2(2\theta_{13}) < 0.13$.

The angles appear in the equations below in many forms. They most often appear as $\sin^2(2\theta)$. The Listings currently use this convention.

Accelerator neutrino experiments: Ignoring the small Δm^2_{21} scale, CP violation, and matter effects, the equations for the probability of appearance in an accelerator oscillation experiment are:

$$P(\nu_\mu \to \nu_\tau) = \sin^2(2\theta_{23})\cos^4(\theta_{13})\sin^2(\Delta m^2_{32}L/4E) \quad (1)$$
$$P(\nu_\mu \to \nu_e) = \sin^2(2\theta_{13})\sin^2(\theta_{23})\sin^2(\Delta m^2_{32}L/4E) \quad (2)$$
$$P(\nu_e \to \nu_\mu) = \sin^2(2\theta_{13})\sin^2(\theta_{23})\sin^2(\Delta m^2_{32}L/4E) \quad (3)$$
$$P(\nu_e \to \nu_\tau) = \sin^2(2\theta_{13})\cos^2(\theta_{23})\sin^2(\Delta m^2_{32}L/4E) \quad (4)$$

For the case of negligible θ_{13}, these probabilities vanish except for $\mathrm{P}(\nu_\mu \to \nu_\tau)$, which then takes the familiar two-neutrino form.

New long-baseline experiments are being planned to search for non-zero θ_{13} through $P(\nu_\mu \to \nu_e)$. Including the CP violating terms and low mass scale, the equation for neutrino oscillation in vacuum is:

$$\begin{aligned} P(\nu_\mu \to \nu_e) &= P1 + P2 + P3 + P4 \\ P1 &= \sin^2(\theta_{23})\sin^2(2\theta_{13})\sin^2(\Delta m^2_{32}L/4E) \\ P2 &= \cos^2(\theta_{23})\sin^2(2\theta_{13})\sin^2(\Delta m^2_{21}L/4E) \\ P3 &= -/+ J\sin(\delta)\sin(\Delta m^2_{32}L/4E) \\ P4 &= J\cos(\delta)\cos(\Delta m^2_{32}L/4E) \end{aligned} \quad (5)$$

where

$$J = \cos(\theta_{13})\sin(2\theta_{12})\sin(2\theta_{13})\sin(2\theta_{23})\sin(\Delta m^2_{32}L/4E) \sin(\Delta m^2_{21}L/4E) \qquad (6)$$

is the "Jarlskog Invariant" for the lepton sector, and the sign in the 3rd term is negative for neutrinos and positive for anti-neutrinos. For most new proposed long-baseline accelerator experiments, P2 can safely be neglected, but depending on the values of θ_{13} and δ, the other three terms could be comparable. Also, depending on the distance and the mass hierarchy, matter effects will need to be included.

Reactor neutrino experiments: Nuclear reactors are prolific sources of $\bar{\nu}_e$ with an energy near 4 MeV. The oscillation probability can be expressed

$$P(\bar{\nu}_e \to \bar{\nu}_e) = 1 - \cos^4(\theta_{13})\sin^2(2\theta_{12})\sin^2(\Delta m^2_{21}L/4E) - \sin^2(2\theta_{13})\sin^2(\Delta m^2_{32}L/4E) \qquad (7)$$

For short distances (L<5 km), it is a good approximation to ignore the second term on the right, and this takes the familiar two-neutrino form with θ_{13} and Δm^2_{32}. For long distances and small θ_{13}, the last term oscillates rapidly and averages to zero for an experiment with finite energy resolution, leading to the familiar two-neutrino form with θ_{12} and Δm^2_{21}.

Solar and Atmospheric neutrino experiments: Solar neutrino experiments are sensitive to ν_e disappearance and have allowed the measurement of θ_{12} and Δm^2_{21}. They are also sensitive to θ_{13}. In the discussion after Eq. (13.21), we identify $\Delta m^2_{\odot} = \Delta m^2_{21}$ and $\theta_{\odot} = \theta_{12}$.

Atmospheric neutrino experiments are primarily sensitive to ν_μ disappearance through $\nu_\mu \to \nu_\tau$ oscillations, and have

allowed the measurement of θ_{23} and Δm^2_{32}. In Eqs. (13.24) and (13.25), we identify $\Delta m^2_{atm} = \Delta m^2_{32} \sim \Delta m^2_{31}$ and $\theta_{atm} = \theta_{23}$. Despite the large ν_e component of the atmospheric neutrino flux, it is difficult to measure Δm^2_{21} effects. This is because of a cancellation between $\nu_\mu \to \nu_e$ and $\nu_e \to \nu_\mu$ together, with the fact that the ratio of ν_μ and ν_e atmospheric fluxes, which arise from sequential π and μ decay, is near 2.

$\sin^2(2\theta_{12})$

VALUE	DOCUMENT ID		TECN	COMMENT
$0.86^{+0.03}_{-0.04}$	[55] AHARMIM	05A	FIT	KamLAND + global solar
• • • We do not use the following data for averages, fits, limits, etc. • • •				
0.75–0.95	[56] AHARMIM	05A	FIT	global solar
0.82 ± 0.05	[57] ARAKI	05	FIT	KamLAND + global solar
0.82 ± 0.04	[58] AHMED	04A	FIT	KamLAND + global solar
0.71–0.93	[59] AHMED	04A	FIT	global solar
$0.85^{+0.05}_{-0.07}$	[60] SMY	04	FIT	KamLAND + global solar
$0.83^{+0.06}_{-0.08}$	[61] SMY	04	FIT	global solar
$0.87^{+0.07}_{-0.08}$	[62] SMY	04	FIT	SKAM + SNO
0.62–0.88	[63] AHMAD	02B	FIT	global solar
0.62–0.95	[64] FUKUDA	02	FIT	global solar

[55] The result given by AHARMIM 05A is $\theta = (33.9 \pm 1.6)^\circ$. This result is obtained by a two-neutrino oscillation analysis using solar neutrino and KamLAND data (ARAKI 05). *CPT* invariance is assumed. AHARMIM 05A also quotes $\theta = (33.9^{+2.4}_{-2.2})^\circ$ as the error enveloping the 68% CL two-dimensional region. This translates into $\sin^2 2\,\theta = 0.86^{+0.05}_{-0.06}$.

[56] AHARMIM 05A obtained this result by a two-neutrino oscillation analysis using the data from all solar neutrino experiments. The listed range of the parameter envelops the 95% CL two-dimensional region shown in figure 35a of AHARMIM 05A. AHARMIM 05A also quotes $\tan^2\theta = 0.45^{+0.09}_{-0.08}$ as the error enveloping the 68% CL two-dimensional region. This translates into $\sin^2 2\,\theta = 0.86^{+0.05}_{-0.07}$.

[57] ARAKI 05 obtained this result by a two-neutrino oscillation analysis using KamLAND and solar neutrino data. *CPT* invariance is assumed. The 1σ error shown here is translated from the number provided by the KamLAND collaboration, $\tan^2\theta = 0.40^{+0.07}_{-0.05}$. The corresponding number quoted in ARAKI 05 is $\tan^2\theta = 0.40^{+0.10}_{-0.07}$ ($\sin^2 2\,\theta = 0.82 \pm 0.07$), which envelops the 68% CL two-dimensional region.

[58] The result given by AHMED 04A is $\theta = (32.5^{+1.7}_{-1.6})^\circ$. This result is obtained by a two-neutrino oscillation analysis using solar neutrino and KamLAND data (EGUCHI 03). *CPT* invariance is assumed. AHMED 04A also quotes $\theta = (32.5^{+2.4}_{-2.3})^\circ$ as the error enveloping the 68% CL two-dimensional region. This translates into $\sin^2 2\,\theta = 0.82 \pm 0.06$.

[59] AHMED 04A obtained this result by a two-neutrino oscillation analysis using the data from all solar neutrino experiments. The listed range of the parameter envelops the 95% CL two-dimensional region shown in Fig. 5(a) of AHMED 04A. The best-fit point is $\Delta(m^2) = 6.5 \times 10^{-5}$ eV^2, $\tan^2\theta = 0.40$ ($\sin^2 2\,\theta = 0.82$).

[60] The result given by SMY 04 is $\tan^2\theta = 0.44 \pm 0.08$. This result is obtained by a two-neutrino oscillation analysis using solar neutrino and KamLAND data (IANNI 03). *CPT* invariance is assumed.

[61] SMY 04 obtained this result by a two-neutrino oscillation analysis using the data from all solar neutrino experiments. The 1σ errors are read from Fig. 6(a) of SMY 04.

[62] SMY 04 obtained this result by a two-neutrino oscillation analysis using the Super-Kamiokande and SNO (AHMAD 02 and AHMAD 02B) solar neutrino data. The 1σ errors are read from Fig. 6(a) of SMY 04.

[63] AHMAD 02B obtained this result by a two-neutrino oscillation analysis using the data from all solar neutrino experiments. The listed range of the parameter envelops the 95% CL two-dimensional region shown in Fig. 4(b) of AHMAD 02B. The best fit point is $\Delta(m^2) = 5.0 \times 10^{-5}$ eV^2 and $\tan\theta = 0.34$ ($\sin^2 2\,\theta = 0.76$).

[64] FUKUDA 02 obtained this result by a two-neutrino oscillation analysis using the data from all solar neutrino experiments. The listed range of the parameter envelops the 95% CL two-dimensional region shown in Fig. 4 of FUKUDA 02. The best fit point is $\Delta(m^2) = 6.9 \times 10^{-5}$ eV^2 and $\tan^2\theta = 0.38$ ($\sin^2 2\,\theta = 0.80$).

Δm^2_{21}

VALUE (10^{-5} eV^2)	*DOCUMENT ID*		*TECN*	*COMMENT*
$8.0^{+0.4}_{-0.3}$	[65] AHARMIM	05A	FIT	KamLAND + global solar
• • • We do not use the following data for averages, fits, limits, etc. • • •				
3.3–14.4	[66] AHARMIM	05A	FIT	global solar
$7.9^{+0.4}_{-0.3}$	[67] ARAKI	05	FIT	KamLAND + global solar
$7.1^{+1.0}_{-0.3}$	[68] AHMED	04A	FIT	KamLAND + global solar
3.2–13.7	[69] AHMED	04A	FIT	global solar
$7.1^{+0.6}_{-0.5}$	[70] SMY	04	FIT	KamLAND + global solar
$6.0^{+1.7}_{-1.6}$	[71] SMY	04	FIT	global solar
$6.0^{+2.5}_{-1.6}$	[72] SMY	04	FIT	SKAM + SNO
2.8–12.0	[73] AHMAD	02B	FIT	global solar
3.2–19.1	[74] FUKUDA	02	FIT	global solar

[65] AHARMIM 05A obtained this result by a two-neutrino oscillation analysis using solar neutrino and KamLAND data (ARAKI 05). *CPT* invariance is assumed. AHARMIM 05A also quotes $\Delta(m^2) = (8.0^{+0.6}_{-0.4}) \times 10^{-5}$ eV^2 as the error enveloping the 68% CL two-dimensional region.

[66] AHARMIM 05A obtained this result by a two-neutrino oscillation analysis using the data from all solar neutrino experiments. The listed range of the parameter envelops the 95% CL two-dimensional region shown in figure 35a of AHARMIM 05A. AHARMIM 05A also quotes $\Delta(m^2) = (6.5^{+4.4}_{-2.3}) \times 10^{-5}$ eV^2 as the error enveloping the 68% CL two-dimensional region.

[67] ARAKI 05 obtained this result by a two-neutrino oscillation analysis using KamLAND and solar neutrino data. *CPT* invariance is assumed. The 1σ error shown here is provided by the KamLAND collaboration. The error quoted in ARAKI 05, $\Delta(m^2) = (7.9^{+0.6}_{-0.5}) \times 10^{-5}$, envelops the 68% CL two-dimensional region.

[68] AHMED 04A obtained this result by a two-neutrino oscillation analysis using solar neutrino and KamLAND data (EGUCHI 03). *CPT* invariance is assumed. AHMED 04A also quotes $\Delta(m^2) = (7.1^{+1.2}_{-0.6}) \times 10^{-5}$ eV^2 as the error enveloping the 68% CL two-dimensional region.

[69] AHMED 04A obtained this result by a two-neutrino oscillation analysis using the data from all solar neutrino experiments. The listed range of the parameter envelops the 95% CL two-dimensional region shown in Fig. 5(a) of AHMED 04A. The best-fit point is $\Delta(m^2) = 6.5 \times 10^{-5}$ eV^2, tan$^2\theta = 0.40$ (sin$^2 2\,\theta = 0.82$).

[70] SMY 04 obtained this result by a two-neutrino oscillation analysis using solar neutrino and KamLAND data (IANNI 03). *CPT* invariance is assumed.

[71] SMY 04 obtained this result by a two-neutrino oscillation analysis using the data from all solar neutrino experiments. The 1σ errors are read from Fig. 6(a) of SMY 04.

[72] SMY 04 obtained this result by a two-neutrino oscillation analysis using the Super-Kamiokande and SNO (AHMAD 02 and AHMAD 02B) solar neutrino data. The 1σ errors are read from Fig. 6(a) of SMY 04.

[73] AHMAD 02B obtained this result by a two-neutrino oscillation analysis using the data from all solar neutrino experiments. The listed range of the parameter envelops the 95% CL two-dimensional region shown in Fig. 4(b) of AHMAD 02B. The best fit point is $\Delta(m^2) = 5.0 \times 10^{-5}$ eV^2 and tan$\theta = 0.34$ (sin$^2 2\,\theta = 0.76$).

[74] FUKUDA 02 obtained this result by a two-neutrino oscillation analysis using the data from all solar neutrino experiments. The listed range of the parameter envelops the 95% CL two-dimensional region shown in Fig. 4 of FUKUDA 02. The best fit point is $\Delta(m^2) = 6.9 \times 10^{-5}$ eV^2 and tan$^2\theta = 0.38$ (sin$^2 2\,\theta = 0.80$).

sin$^2(2\theta_{23})$

The ranges below correspond to the projection onto the sin$^2(2\theta_{23})$ axis of the 90% CL contours in the sin$^2(2\theta_{23})$ – Δm^2_{32} plane presented by the authors.

VALUE	*DOCUMENT ID*		*TECN*	*COMMENT*
>0.92	[75] ASHIE	05	SKAM	Super-Kamiokande
• • • We do not use the following data for averages, fits, limits, etc. • • •				
>0.58	[76] ALIU	05	K2K	KEK to Super-K
>0.6	[77] ALLISON	05	SOU2	
>0.80	[78] AMBROSIO	04	MCRO	MACRO
>0.90	[79] ASHIE	04	SKAM	L/E distribution
>0.30	[80] AHN	03	K2K	KEK to Super-K
>0.45	[81] AMBROSIO	03	MCRO	MACRO
>0.77	[82] AMBROSIO	03	MCRO	MACRO
>0.50	[83] SANCHEZ	03	SOU2	Soudan-2 Atmospheric
>0.80	[84] AMBROSIO	01	MCRO	upward μ
>0.82	[85] AMBROSIO	01	MCRO	upward μ
>0.45	[86] FUKUDA	99C	SKAM	upward μ
>0.70	[87] FUKUDA	99D	SKAM	upward μ
>0.30	[88] FUKUDA	99D	SKAM	stop μ / through
>0.82	[89] FUKUDA	98C	SKAM	Super-Kamiokande
>0.30	[90] HATAKEYAMA	98	KAMI	Kamiokande
>0.73	[91] HATAKEYAMA	98	KAMI	Kamiokande
>0.65	[92] FUKUDA	94	KAMI	Kamiokande

[75] ASHIE 05 obtained this result by a two-neutrino oscillation analysis using 92 kton yr atmospheric neutrino data from the complete Super-Kamiokande I running period.

[76] The best fit is for maximal mixing.

[77] ALLISON 05 result is based upon atmospheric neutrino interactions including upward-stopping muons, with an exposure of 5.9 kton yr. From a two-flavor oscillation analysis the best-fit point is $\Delta m^2 = 0.0017$ eV^2 and $\sin^2(2\theta) = 0.97$.

[78] AMBROSIO 04 obtained this result, without using the absolute normalization of the neutrino flux, by combining the angular distribution of upward through-going muon tracks with $E_\mu > 1$ GeV, N_{low} and N_{high}, and the numbers of InDown + UpStop and InUp events. Here, N_{low} and N_{high} are the number of events with reconstructed neutrino energies < 30 GeV and > 130 GeV, respectively. InDown and InUp represent events with downward and upward-going tracks starting inside the detector due to neutrino interactions, while UpStop represents entering upward-going tracks which stop in the detector. The best fit is for maximal mixing.

[79] ASHIE 04 obtained this result from the L(flight length)/E(estimated neutrino energy) distribution of ν_μ disappearance probability, using the Super-Kamiokande-I 1489 live-day atmospheric neutrino data.

[80] There are several islands of allowed region from this K2K analysis, extending to high values of Δm^2. We only include the one that overlaps atmospheric neutrino analyses. The best fit is for maximal mixing.

[81] AMBROSIO 03 obtained this result on the basis of the ratio $R = N_{low}/N_{high}$, where N_{low} and N_{high} are the number of upward through-going muon events with reconstructed neutrino energy < 30 GeV and > 130 GeV, respectively. The data came from the full detector run started in 1994. The method of FELDMAN 98 is used to obtain the limits.

[82] AMBROSIO 03 obtained this result by using the ratio R and the angular distribution of the upward through-going muons. R is given in the previous note and the angular distribution is reported in AMBROSIO 01. The method of FELDMAN 98 is used to obtain the limits. The best fit is to maximal mixing.

[83] SANCHEZ 03 is based on an exposure of 5.9 kton yr. The result is obtained using a likelihood analysis of the neutrino L/E distribution for a selection μ flavor sample while the *e*-flavor sample provides flux normalization. The method of FELDMAN 98 is used to obtain the allowed region. The best fit is $\sin^2(2\theta) = 0.97$.

[84] AMBROSIO 01 result is based on the angular distribution of upward through-going muon tracks with $E_\mu > 1$ GeV. The data came from three different detector configurations, but the statistics is largely dominated by the full detector run, from May 1994 to December 2000. The total live time, normalized to the full detector configuration is 6.17 years. The best fit is obtained outside the physical region. The method of FELDMAN 98 is used to obtain the limits. The best fit is for maximal mixing.

[85] AMBROSIO 01 result is based on the angular distribution and normalization of upward through-going muon tracks with $E_\mu > 1$ GeV. See the previous footnote.

[86] FUKUDA 99C obtained this result from a total of 537 live days of upward through-going muon data in Super-Kamiokande between April 1996 to January 1998. With a threshold of $E_\mu > 1.6$ GeV, the observed flux is $(1.74 \pm 0.07 \pm 0.02) \times 10^{-13}$ cm^{-2}s^{-1}sr^{-1}. The best fit is $\sin^2(2\theta) = 0.95$.

[87] FUKUDA 99D obtained this result from a simultaneous fitting to zenith angle distributions of upward-stopping and through-going muons. The flux of upward-stopping muons of minimum energy of 1.6 GeV measured between April 1996 and January 1998 is $(0.39 \pm 0.04 \pm 0.02) \times 10^{-13}$ cm^{-2}s^{-1}sr^{-1}. This is compared to the expected flux of $(0.73 \pm 0.16$ (theoretical error)$) \times 10^{-13}$ cm^{-2}s^{-1}sr^{-1}. The best fit is to maximal mixing.

[88] FUKUDA 99D obtained this result from the zenith dependence of the upward-stopping/through-going flux ratio. The best fit is to maximal mixing.

[89] FUKUDA 98C obtained this result by an analysis of 33.0 kton yr atmospheric neutrino data. The best fit is for maximal mixing.

[90] HATAKEYAMA 98 obtained this result from a total of 2456 live days of upward-going muon data in Kamiokande between December 1985 and May 1995. With a threshold of $E_\mu > 1.6$ GeV, the observed flux of upward through-going muons is $(1.94 \pm 0.10^{+0.07}_{-0.06}) \times 10^{-13}$ cm^{-2}s^{-1}sr^{-1}. This is compared to the expected flux of $(2.46 \pm 0.54$ (theoretical error)$) \times 10^{-13}$ cm^{-2}s^{-1}sr^{-1}. The best fit is for maximal mixing.

[91] HATAKEYAMA 98 obtained this result from a combined analysis of Kamiokande contained events (FUKUDA 94) and upward going muon events. The best fit is $\sin^2(2\theta) = 0.95$.

[92] FUKUDA 94 obtained the result by a combined analysis of sub- and multi-GeV atmospheric neutrino events in Kamiokande. The best fit is for maximal mixing.

Δm^2_{32}

The sign of Δm^2_{32} is not known at this time. Only the absolute value is quoted below. The ranges below correspond to the projection onto the Δm^2_{32} axis of the 90% CL contours in the $\sin^2(2\theta_{23}) - \Delta m^2_{32}$ plane presented by the authors.

VALUE (10^{-3} eV^2)	*DOCUMENT ID*		*TECN*	*COMMENT*
1.9 to 3.0	[93] ASHIE	04	SKAM	L/E distribution
• • • We do not use the following data for averages, fits, limits, etc. • • •				
1.9–3.6	[94] ALIU	05	K2K	KEK to Super-K
0.3–12	[95] ALLISON	05	SOU2	
1.5–3.4	[96] ASHIE	05	SKAM	atmospheric neutrino
0.6–8.0	[97] AMBROSIO	04	MCRO	MACRO
1.5–3.9	[98] AHN	03	K2K	KEK to Super-K
0.25–9.0	[99] AMBROSIO	03	MCRO	MACRO
0.6–7.0	[100] AMBROSIO	03	MCRO	MACRO
0.15–15	[101] SANCHEZ	03	SOU2	Soudan-2 Atmospheric
0.6–15	[102] AMBROSIO	01	MCRO	upward μ
1.0–6.0	[103] AMBROSIO	01	MCRO	upward μ
1.0–50	[104] FUKUDA	99C	SKAM	upward μ
1.5–15.0	[105] FUKUDA	99D	SKAM	upward μ
0.7–18	[106] FUKUDA	99D	SKAM	stop μ / through
0.5–6.0	[107] FUKUDA	98C	SKAM	Super-Kamiokande
0.55–50	[108] HATAKEYAMA	98	KAMI	Kamiokande
4–23	[109] HATAKEYAMA	98	KAMI	Kamiokande
5–25	[110] FUKUDA	94	KAMI	Kamiokande

[93] ASHIE 04 obtained this result from the L(flight length)/E(estimated neutrino energy) distribution of ν_μ disappearance probability, using the Super-Kamiokande-I 1489 live-day atmospheric neutrino data. The best fit is for $\Delta m^2 = 2.4 \times 10^{-3}$ eV^2.

[94] The best fit in the physical region is for $\Delta m^2 = 2.8 \times 10^{-3}$ eV^2.

[95] ALLISON 05 result is based on an atmospheric neutrino observation with an exposure of 5.9 kton yr. From a two-flavor oscillation analysis the best-fit point is $\Delta m^2 = 0.0017$ eV^2 and $\sin^2 2\,\theta = 0.97$.

[96] ASHIE 05 obtained this result by a two-neutrino oscillation analysis using 92 kton yr atmospheric neutrino data from the complete Super-Kamiokande I running period. The best fit is for $\Delta m^2 = 2.1 \times 10^{-3}$ eV^2.

[97] AMBROSIO 04 obtained this result, without using the absolute normalization of the neutrino flux, by combining the angular distribution of upward through-going muon tracks with $E_\mu > 1$ GeV, N_{low} and N_{high}, and the numbers of InDown + UpStop and InUp events. Here, N_{low} and N_{high} are the number of events with reconstructed neutrino energies < 30 GeV and > 130 GeV, respectively. InDown and InUp represent events with downward and upward-going tracks starting inside the detector due to neutrino interactions, while UpStop represents entering upward-going tracks which stop in the detector. The best fit is for $\Delta m^2 = 2.3 \times 10^{-3}$ eV^2.

[98] There are several islands of allowed region from this K2K analysis, extending to high values of Δm^2. We only include the one that overlaps atmospheric neutrino analyses. The best fit is for $\Delta m^2 = 2.8 \times 10^{-3}$ eV^2.

[99] AMBROSIO 03 obtained this result on the basis of the ratio $R = N_{low}/N_{high}$, where N_{low} and N_{high} are the number of upward through-going muon events with reconstructed neutrino energy < 30 GeV and > 130 GeV, respectively. The data came from the full detector run started in 1994. The method of FELDMAN 98 is used to obtain the limits. The best fit is for $\Delta m^2 = 2.5 \times 10^{-3}$ eV^2.

[100] AMBROSIO 03 obtained this result by using the ratio R and the angular distribution of the upward through-going muons. R is given in the previous note and the angular distribution is reported in AMBROSIO 01. The method of FELDMAN 98 is used to obtain the limits. The best fit is for $\Delta m^2 = 2.5 \times 10^{-3}$ eV^2.

[101] SANCHEZ 03 is based on an exposure of 5.9 kton yr. The result is obtained using a likelihood analysis of the neutrino L/E distribution for a selection μ flavor sample while the *e*-flavor sample provides flux normalization. The method of FELDMAN 98 is used to obtain the allowed region. The best fit is for $\Delta m^2 = 5.2 \times 10^{-3}$ eV^2.

[102] AMBROSIO 01 result is based on the angular distribution of upward through-going muon tracks with $E_\mu > 1$ GeV. The data came from three different detector configurations, but the statistics is largely dominated by the full detector run, from May 1994 to December 2000. The total live time, normalized to the full detector configuration is 6.17 years. The best fit is obtained outside the physical region. The method of FELDMAN 98 is used to obtain the limits.

[103] AMBROSIO 01 result is based on the angular distribution and normalization of upward through-going muon tracks with $E_\mu > 1$ GeV. See the previous footnote.

[104] FUKUDA 99C obtained this result from a total of 537 live days of upward through-going muon data in Super-Kamiokande between April 1996 to January 1998. With a threshold of $E_\mu > 1.6$ GeV, the observed flux is $(1.74 \pm 0.07 \pm 0.02) \times 10^{-13}$ cm^{-2}s^{-1}sr^{-1}. The best fit is for $\Delta m^2 = 5.9 \times 10^{-3}$ eV^2.

[105] FUKUDA 99D obtained this result from a simultaneous fitting to zenith angle distributions of upward-stopping and through-going muons. The flux of upward-stopping muons of minimum energy of 1.6 GeV measured between April 1996 and January 1998 is $(0.39 \pm 0.04 \pm 0.02) \times 10^{-13}$ cm^{-2}s^{-1}sr^{-1}. This is compared to the expected flux of $(0.73 \pm 0.16$ (theoretical error)$) \times 10^{-13}$ cm^{-2}s^{-1}sr^{-1}. The best fit is for $\Delta m^2 = 3.9 \times 10^{-3}$ eV^2.

[106] FUKUDA 99D obtained this result from the zenith dependence of the upward-stopping/through-going flux ratio. The best fit is for $\Delta m^2 = 3.1 \times 10^{-3}$ eV^2.

[107] FUKUDA 98C obtained this result by an analysis of 33.0 kton yr atmospheric neutrino data. The best fit is for $\Delta m^2 = 2.2 \times 10^{-3}$ eV^2.

[108] HATAKEYAMA 98 obtained this result from a total of 2456 live days of upward-going muon data in Kamiokande between December 1985 and May 1995. With a threshold of $E_\mu > 1.6$ GeV, the observed flux of upward through-going muons is $(1.94 \pm 0.10^{+0.07}_{-0.06}) \times 10^{-13}$ cm^{-2}s^{-1}sr^{-1}. This is compared to the expected flux of $(2.46 \pm 0.54$ (theoretical error)$) \times 10^{-13}$ cm^{-2}s^{-1}sr^{-1}. The best fit is for $\Delta m^2 = 2.2 \times 10^{-3}$ eV^2.

[109] HATAKEYAMA 98 obtained this result from a combined analysis of Kamiokande contained events (FUKUDA 94) and upward going muon events. The best fit is for $\Delta m^2 = 13 \times 10^{-3}$ eV^2.

[110] FUKUDA 94 obtained the result by a combined analysis of sub- and multi-GeV atmospheric neutrino events in Kamiokande. The best fit is for $\Delta m^2 = 16 \times 10^{-3}$ eV^2.

$\sin^2(2\theta_{13})$

At present time, limits of $\sin^2(2\ \theta_{13})$ are derived from the search for the reactor $\overline{\nu}_e$ disappearance at distances corresponding to the Δm^2_{23} value, i.e. L $\sim$ 1km. Alternatively, somewhat weaker limits can be obtained from the analysis of the solar neutrino data.

VALUE	*CL%*	*DOCUMENT ID*		*TECN*	*COMMENT*
<0.19	90	[111] APOLLONIO	99	CHOZ	Reactor Experiment
• • • We do not use the following data for averages, fits, limits, etc. • • •					
<0.48	90	[112] AHN	04	K2K	Accelerator experiment
<0.36	90	[113] BOEHM	01		Palo Verde react.
<0.45	90	[114] BOEHM	00		Palo Verde react.

[111] The quoted limit is for $\Delta m^2_{32} = 1.9 \times 10^{-3}$ eV^2. That value of Δm^2_{32} is the 1-σ low value for ALIU 05. For the ALIU 05 best fit value of 2.8×10^{-3} eV^2, the $\sin^2 2\ \theta_{13}$ limit is < 0.13. See also APOLLONIO 03 for a detailed description of the experiment.

[112] AHN 04 searched for $\nu_\mu \rightarrow \nu_e$ appearance. Assuming $2\ \sin^2(2\ \theta_{\mu_e}) = \sin^2(2\ \theta_{13})$, a limit on $\sin^2(2\ \theta_{\mu_e})$ is converted to a limit on $\sin^2(2\ \theta_{13})$.The quoted limit is for $\Delta m^2_{32} = 1.9 \times 10^{-3}$ eV^2. That value of Δm^2_{32} is the one-σ low value for ALIU 05. For the ALIU 05 best fit value of 2.8×10^{-3} eV^2, the $\sin^2(2\ \theta_{13})$ limit is < 0.30.

[113] The quoted limit is for $\Delta m^2_{32} = 1.9 \times 10^{-3}$ eV^2. That value of Δm^2_{32} is the 1-σ low value for ALIU 05. For the ALIU 05 best fit value of 2.8×10^{-3} eV^2, the $\sin^2 2\ \theta_{13}$ limit is < 0.19. In this range, the θ_{13} limit is larger for lower values of Δm^2_{32}, and smaller for higher values of Δm^2_{32}.

[114] The quoted limit is for $\Delta m^2_{32} = 1.9 \times 10^{-3}$ eV^2. That value of Δm^2_{32} is the 1-σ low value for ALIU 05. For the ALIU 05 best fit value of 2.8×10^{-3} eV^2, the $\sin^2 2\ \theta_{13}$ limit is < 0.23.

(C) Other neutrino mixing results

The LSND collaboration reported in AGUILAR 01 a signal which is consistent with $\overline{\nu}_\mu \rightarrow \overline{\nu}_e$ oscillations. In a three neutrino framework, this would be a measurement of θ_{12} and Δm^2_{21}. This does not appear to be consistent with the interpretation of other neutrino data, particularly solar neutrino experiments. If the LSND anomaly is correct, a more complicated framework is required, perhaps involving one or more sterile neutrinos, or even CPT violation. The following listings include results which might be relevant towards understanding or ruling out the LSND observations. They include searches for $\nu_\mu \rightarrow \nu_e$, $\overline{\nu}_\mu \rightarrow \overline{\nu}_e$, sterile neutrino oscillations, and *CPT* violation.

$\Delta(m^2)$ for $\sin^2(2\theta) = 1$ $(\nu_\mu \rightarrow \nu_e)$

VALUE (eV^2)	*CL%*	*DOCUMENT ID*		*TECN*	*COMMENT*
• • • We do not use the following data for averages, fits, limits, etc. • • •					
<0.0008	90	AHN	04	K2K	Water Cherenkov
<0.4	90	ASTIER	03	NOMD	CERN SPS
<2.4	90	AVVAKUMOV	02	NTEV	NUTEV FNAL
		[115] AGUILAR	01	LSND	$\nu\mu \rightarrow \nu_e$ osc.prob.
0.03 to 0.3	95	[116] ATHANASSO...98		LSND	$\nu_\mu \rightarrow \nu_e$
<2.3	90	[117] LOVERRE	96		CHARM/CDHS
<0.9	90	VILAIN	94C	CHM2	CERN SPS
<0.09	90	ANGELINI	86	HLBC	BEBC CERN PS

[115] AGUILAR 01 is the final analysis of the LSND full data set. Search is made for the $\nu_\mu \rightarrow \nu_e$ oscillations using ν_μ from π^+ decay in flight by observing beam-on electron events from $\nu_e C \rightarrow e^- X$. Present analysis results in $8.1 \pm 12.2 \pm 1.7$ excess events in the $60 < E_e < 200$ MeV energy range, corresponding to oscillation probability of $0.10 \pm 0.16 \pm 0.04\%$. This is consistent, though less significant, with the previous result of ATHANASSOPOULOS 98, which it supersedes. The present analysis uses selection criteria developed for the decay at rest region, and is less effective in removing the background above 60 MeV than ATHANASSOPOULOS 98.

[116] ATHANASSOPOULOS 98 is a search for the $\nu_\mu \rightarrow \nu_e$ oscillations using ν_μ from π^+ decay in flight. The 40 observed beam-on electron events are consistent with $\nu_e C \rightarrow e^- X$; the expected background is 21.9 ± 2.1. Authors interpret this excess as evidence for an oscillation signal corresponding to oscillations with probability $(0.26 \pm 0.10 \pm 0.05)\%$. Although the significance is only $2.3\,\sigma$, this measurement is an important and consistent cross check of ATHANASSOPOULOS 96 who reported evidence for $\overline{\nu}_\mu \rightarrow \overline{\nu}_e$ oscillations from μ^+ decay at rest. See also ATHANASSOPOULOS 98B.

[117] LOVERRE 96 uses the charged-current to neutral-current ratio from the combined CHARM (ALLABY 86) and CDHS (ABRAMOWICZ 86) data from 1986.

$\sin^2(2\theta)$ for "Large" $\Delta(m^2)$ $(\nu_\mu \rightarrow \nu_e)$

VALUE (units 10^{-3})	*CL%*	*DOCUMENT ID*		*TECN*	*COMMENT*
• • • We do not use the following data for averages, fits, limits, etc. • • •					
<110	90	[118] AHN	04	K2K	Water Cherenkov
< 1.4	90	ASTIER	03	NOMD	CERN SPS
< 1.6	90	AVVAKUMOV	02	NTEV	NUTEV FNAL
		[119] AGUILAR	01	LSND	$\nu\mu \rightarrow \nu_e$ osc.prob.
0.5 to 30	95	[120] ATHANASSO...98		LSND	$\nu_\mu \rightarrow \nu_e$
< 3.0	90	[121] LOVERRE	96		CHARM/CDHS
< 9.4	90	VILAIN	94C	CHM2	CERN SPS
< 5.6	90	[122] VILAIN	94C	CHM2	CERN SPS

[118] The limit becomes $\sin^2 2\theta < 0.15$ at $\Delta m^2 = 2.8 \times 10^{-3}$ eV^2, the bets-fit value of the ν_μ disappearance analysis in K2K.

[119] AGUILAR 01 is the final analysis of the LSND full data set of the search for the $\nu_\mu \rightarrow \nu_e$ oscillations. See footnote in preceding table for further details.

[120] ATHANASSOPOULOS 98 report $(0.26 \pm 0.10 \pm 0.05)\%$ for the oscillation probability; the value of $\sin^2 2\theta$ for large Δm^2 is deduced from this probability. See footnote in preceding table for further details, and see the paper for a plot showing allowed regions. If effect is due to oscillation, it is most likely to be intermediate $\sin^2 2\theta$ and Δm^2. See also ATHANASSOPOULOS 98B.

[121] LOVERRE 96 uses the charged-current to neutral-current ratio from the combined CHARM (ALLABY 86) and CDHS (ABRAMOWICZ 86) data from 1986.

[122] VILAIN 94C limit derived by combining the ν_μ and $\overline{\nu}_\mu$ data assuming *CP* conservation.

$\Delta(m^2)$ for $\sin^2(2\theta) = 1$ $(\overline{\nu}_\mu \rightarrow \overline{\nu}_e)$

VALUE (eV^2)	*CL%*	*DOCUMENT ID*		*TECN*	*COMMENT*
• • • We do not use the following data for averages, fits, limits, etc. • • •					
<0.055	90	[123] ARMBRUSTER	02	KAR2	Liquid Sci. calor.
<2.6	90	AVVAKUMOV	02	NTEV	NUTEV FNAL
0.03–0.05		[124] AGUILAR	01	LSND	LAMPF
0.05–0.08	90	[125] ATHANASSO...	96	LSND	LAMPF
0.048–0.090	80	[126] ATHANASSO...	95		
<0.07	90	[127] HILL	95		
<0.9	90	VILAIN	94C	CHM2	CERN SPS
<0.14	90	[128] FREEDMAN	93	CNTR	LAMPF

[123] ARMBRUSTER 02 is the final analysis of the KARMEN 2 data for 17.7 m distance from the ISIS stopped pion and muon neutrino source. It is a search for $\overline{\nu}_e$, detected by the inverse β-decay reaction on protons and ^{12}C. 15 candidate events are observed, and 15.8 ± 0.5 background events are expected, hence no oscillation signal is detected. The results exclude large regions of the parameter area favored by the LSND experiment.

[124] AGUILAR 01 is the final analysis of the LSND full data set. It is a search for $\overline{\nu}_e$ 30 m from LAMPF beam stop. Neutrinos originate mainly for π^+ decay at rest. $\overline{\nu}_e$ are detected through $\overline{\nu}_e p \rightarrow e^+ n$ ($20 < E_{e^+} < 60$ MeV) in delayed coincidence with $np \rightarrow d\gamma$. AUthors observe 87.9 ± 22.4 ± 6.0 total excess events. The observation is attributed to $\overline{\nu}_\mu \rightarrow \overline{\nu}_e$ oscillations with the oscillation probability of 0.264 ± 0.067 ± 0.045%, consistent with the previously published result. Taking into account all constraints, the most favored allowed region of oscillation parameters is a band of $\Delta(m^2)$ from 0.2–2.0 eV^2. Supersedes ATHANASSOPOULOS 95, ATHANASSOPOULOS 96, and ATHANASSOPOULOS 98.

[125] ATHANASSOPOULOS 96 is a search for $\overline{\nu}_e$ 30 m from LAMPF beam stop. Neutrinos originate mainly from π^+ decay at rest. $\overline{\nu}_e$ could come from either $\overline{\nu}_\mu \rightarrow \overline{\nu}_e$ or $\nu_e \rightarrow \overline{\nu}_e$; our entry assumes the first interpretation. They are detected through $\overline{\nu}_e p \rightarrow e^+ n$ (20 MeV $< E_{e^+} <$60 MeV) in delayed coincidence with $np \rightarrow d\gamma$. Authors observe 51 ± 20 ± 8 total excess events over an estimated background 12.5 ± 2.9. ATHANASSOPOULOS 96B is a shorter version of this paper.

[126] ATHANASSOPOULOS 95 error corresponds to the 1.6σ band in the plot. The expected background is 2.7 ± 0.4 events. Corresponds to an oscillation probability of $(0.34^{+0.20}_{-0.18} \pm 0.07)$%. For a different interpretation, see HILL 95. Replaced by ATHANASSOPOULOS 96.

[127] HILL 95 is a report by one member of the LSND Collaboration, reporting a different conclusion from the analysis of the data of this experiment (see ATHANASSOPOULOS 95). Contrary to the rest of the LSND Collaboration, Hill finds no evidence for the neutrino oscillation $\overline{\nu}_\mu \rightarrow \overline{\nu}_e$ and obtains only upper limits.

[128] FREEDMAN 93 is a search at LAMPF for $\overline{\nu}_e$ generated from any of the three neutrino types ν_μ, $\overline{\nu}_\mu$, and ν_e which come from the beam stop. The $\overline{\nu}_e$'s would be detected by the reaction $\overline{\nu}_e p \rightarrow e^+ n$. FREEDMAN 93 replaces DURKIN 88.

$\sin^2(2\theta)$ for "Large" $\Delta(m^2)$ $(\overline{\nu}_\mu \rightarrow \overline{\nu}_e)$

VALUE (units 10^{-3})	CL%	DOCUMENT ID		TECN	COMMENT
• • • We do not use the following data for averages, fits, limits, etc. • • •					
<1.7	90	[129] ARMBRUSTER	02	KAR2	Liquid Sci. calor.
<1.1	90	AVVAKUMOV	02	NTEV	NUTEV FNAL
5.3±1.3±9.0		[130] AGUILAR	01	LSND	LAMPF
6.2±2.4±1.0		[131] ATHANASSO...	96	LSND	LAMPF
3–12	80	[132] ATHANASSO...	95		
<6	90	[133] HILL	95		

[129] ARMBRUSTER 02 is the final analysis of the KARMEN 2 data. See footnote in the preceding table for further details, and the paper for the exclusion plot.

[130] AGUILAR 01 is the final analysis of the LSND full data set. The deduced oscillation probability is $0.264 \pm 0.067 \pm 0.045\%$; the value of $\sin^2 2\theta$ for large $\Delta(m^2)$ is twice this probability (although these values are excluded by other constraints). See footnote in preceding table for further details, and the paper for a plot showing allowed regions. Supersedes ATHANASSOPOULOS 95, ATHANASSOPOULOS 96, and ATHANASSOPOULOS 98.

[131] ATHANASSOPOULOS 96 reports $(0.31 \pm 0.12 \pm 0.05)\%$ for the oscillation probability; the value of $\sin^2 2\theta$ for large $\Delta(m^2)$ should be twice this probability. See footnote in preceding table for further details, and see the paper for a plot showing allowed regions.

[132] ATHANASSOPOULOS 95 error corresponds to the 1.6σ band in the plot. The expected background is 2.7 ± 0.4 events. Corresponds to an oscillation probability of $(0.34^{+0.20}_{-0.18} \pm 0.07)\%$. For a different interpretation, see HILL 95. Replaced by ATHANASSOPOULOS 96.

[133] HILL 95 is a report by one member of the LSND Collaboration, reporting a different conclusion from the analysis of the data of this experiment (see ATHANASSOPOULOS 95). Contrary to the rest of the LSND Collaboration, Hill finds no evidence for the neutrino oscillation $\overline{\nu}_\mu \rightarrow \overline{\nu}_e$ and obtains only upper limits.

$\Delta(m^2)$ for $\sin^2(2\theta) = 1$ $(\nu_\mu(\overline{\nu}_\mu) \rightarrow \nu_e(\overline{\nu}_e))$

VALUE (eV^2)	CL%	DOCUMENT ID		TECN	COMMENT
<0.075	90	BORODOV...	92	CNTR	BNL E776
• • • We do not use the following data for averages, fits, limits, etc. • • •					
<1.6	90	[134] ROMOSAN	97	CCFR	FNAL

[134] ROMOSAN 97 uses wideband beam with a 0.5 km decay region.

$\sin^2(2\theta)$ for "Large" $\Delta(m^2)$ $(\nu_\mu(\overline{\nu}_\mu) \rightarrow \nu_e(\overline{\nu}_e))$

VALUE (units 10^{-3})	CL%	DOCUMENT ID		TECN	COMMENT
<1.8	90	[135] ROMOSAN	97	CCFR	FNAL
• • • We do not use the following data for averages, fits, limits, etc. • • •					
<3.8	90	[136] MCFARLAND	95	CCFR	FNAL
<3	90	BORODOV...	92	CNTR	BNL E776

[135] ROMOSAN 97 uses wideband beam with a 0.5 km decay region.

[136] MCFARLAND 95 state that "This result is the most stringent to date for $250 < \Delta(m^2) < 450$ eV^2 and also excludes at 90%CL much of the high $\Delta(m^2)$ region favored by the recent LSND observation." See ATHANASSOPOULOS 95 and ATHANASSOPOULOS 96.

Sterile neutrino limits from atmospheric neutrino studies

$\Delta(m^2)$ for $\sin^2(2\theta) = 1$ ($\nu_\mu \rightarrow \nu_s$)

ν_s means ν_τ or any sterile (noninteracting) ν.

VALUE (10^{-5} eV^2)	CL%	DOCUMENT ID		TECN	COMMENT
• • • We do not use the following data for averages, fits, limits, etc. • • •					
<3000 (or <550)	90	[137] OYAMA		89	KAMI Water Cherenkov
< 4.2 or > 54.	90	BIONTA		88	IMB Flux has ν_μ, $\overline{\nu}_\mu$, ν_e, and $\overline{\nu}_e$

[137] OYAMA 89 gives a range of limits, depending on assumptions in their analysis. They argue that the region $\Delta(m^2) = (100\text{–}1000) \times 10^{-5}$ eV^2 is not ruled out by any data for large mixing.

Search for $\nu_\mu \rightarrow \nu_s$

VALUE	DOCUMENT ID		TECN	COMMENT
• • • We do not use the following data for averages, fits, limits, etc. • • •				
	[138] AMBROSIO	01	MCRO	matter effects
	[139] FUKUDA	00	SKAM	neutral currents + matter effects

[138] AMBROSIO 01 tested the pure 2-flavor $\nu_\mu \rightarrow \nu_s$ hypothesis using matter effects which change the shape of the zenith-angle distribution of upward through-going muons. With maximum mixing and $\Delta(m^2)$ around 0.0024 eV^2, the $\nu_\mu \rightarrow \nu_s$ oscillation is disfavored with 99% confidence level with respect to the $\nu_\mu \rightarrow \nu_\tau$ hypothesis.

[139] FUKUDA 00 tested the pure 2-flavor $\nu_\mu \rightarrow \nu_s$ hypothesis using three complementary atmospheric-neutrino data samples. With this hypothesis, zenith-angle distributions are expected to show characteristic behavior due to neutral currents and matter effects. In the $\Delta(m^2)$ and $\sin^2 2\theta$ region preferred by the Super-Kamiokande data, the $\nu_\mu \rightarrow \nu_s$ hypothesis is rejected at the 99% confidence level, while the $\nu_\mu \rightarrow \nu_\tau$ hypothesis consistently fits all of the data sample.

CPT tests

$\langle \Delta m^2_{21} - \Delta \overline{m}^2_{21} \rangle$

VALUE (10^{-4} eV^2)	CL%	DOCUMENT ID		TECN	COMMENT
• • • We do not use the following data for averages, fits, limits, etc. • • •					
<1.1	99.7	[140] DEGOUVEA	05	FIT	solar vs. reactor

[140] DEGOUVEA 05 obtained this bound at the 3σ CL from the KamLAND (ARAKI 05) and solar neutrino data.

REFERENCES FOR Neutrino Mixing

AHARMIM	05A	PR C72 055502	B. Aharmim *et al.*	(SNO Collab.)
ALIU	05	PRL 94 081802	E. Aliu *et al.*	(K2K Collab.)
ALLISON	05	PR D72 052005	W.W.M. Allison *et al.*	(SOUDAN-2 Collab.)
ALTMANN	05	PL B616 174	M. Altmann *et al.*	(GNO Collab.)
ARAKI	05	PRL 94 081801	T. Araki *et al.*	(KamLAND Collab.)
ASHIE	05	PR D71 112005	Y. Ashie *et al.*	(SuperK Collab.)
DEGOUVEA	05	PR D71 093002	A. de Gouvea, C. Pena-Garay	
AHARMIM	04	PR D70 093014	B. Aharmim *et al.*	(SNO Collab.)
AHMED	04A	PRL 92 181301	S.N. Ahmed *et al.*	(SNO Collab.)
AHN	04	PRL 93 051801	M.H. Ahn *et al.*	(K2K)
AMBROSIO	04	EPJ C36 323	M. Ambrosio *et al.*	(MACRO Collab.)
ASHIE	04	PRL 93 101801	Y. Ashie *et al.*	(Super-Kamiokande Collab.)
EGUCHI	04	PRL 92 071301	K. Eguchi *et al.*	(KamLAND Collab.)
SMY	04	PR D69 011104R	M.B. Smy *et al.*	(Super-Kamiokande Collab.)
AHN	03	PRL 90 041801	M.H. Ahn *et al.*	(K2K Collab.)
AMBROSIO	03	PL B566 35	M. Ambrosio *et al.*	(MACRO Collab.)

APOLLONIO	03	EPJ C27 331	M. Apollonio *et al.*	(CHOOZ Collab.)
ASTIER	03	PL B570 19	P. Astier *et al.*	(NOMAD Collab.)
EGUCHI	03	PRL 90 021802	K. Eguchi *et al.*	(KamLAND Collab.)
GANDO	03	PRL 90 171302	Y. Gando *et al.*	(Super-Kamiokande Collab.)
IANNI	03	JPG 29 2107	A. Ianni	(INFN Gran Sasso)
SANCHEZ	03	PR D68 113004	M. Sanchez *et al.*	(Soudan 2 Collab.)
ABDURASHI...	02	JETP 95 181	J.N. Abdurashitov *et al.*	(SAGE Collab.)
		Translated from ZETF 122 211.		
AHMAD	02	PRL 89 011301	Q.R. Ahmad *et al.*	(SNO Collab.)
AHMAD	02B	PRL 89 011302	Q.R. Ahmad *et al.*	(SNO Collab.)
ARMBRUSTER	02	PR D65 112001	B. Armbruster *et al.*	(KARMEN 2 Collab.)
AVVAKUMOV	02	PRL 89 011804	S. Avvakumov *et al.*	(NuTeV Collab.)
FUKUDA	02	PL B539 179	S. Fukuda *et al.*	(Super-Kamiokande Collab.)
AGUILAR	01	PR D64 112007	A. Aguilar *et al.*	(LSND Collab.)
AHMAD	01	PRL 87 071301	Q.R. Ahmad *et al.*	(SNO Collab.)
AMBROSIO	01	PL B517 59	M. Ambrosio *et al.*	(MACRO Collab.)
BOEHM	01	PR D64 112001	F. Boehm *et al.*	
FUKUDA	01	PRL 86 5651	S. Fukuda *et al.*	(Super-Kamiokande Collab.)
AMBROSIO	00	PL B478 5	M. Ambrosio *et al.*	(MACRO Collab.)
BOEHM	00	PRL 84 3764	F. Boehm *et al.*	
FUKUDA	00	PRL 85 3999	S. Fukuda *et al.*	(Super-Kamiokande Collab.)
ABDURASHI...	99B	PR C60 055801	J.N. Abdurashitov *et al.*	(SAGE Collab.)
ALLISON	99	PL B449 137	W.W.M. Allison *et al.*	(Soudan 2 Collab.)
APOLLONIO	99	PL B466 415	M. Apollonio *et al.*	(CHOOZ Collab.)
Also		PL B472 434 (erratum)	M. Apollonio *et al.*	(CHOOZ Collab.)
FUKUDA	99C	PRL 82 2644	Y. Fukuda *et al.*	(Super-Kamiokande Collab.)
FUKUDA	99D	PL B467 185	Y. Fukuda *et al.*	(Super-Kamiokande Collab.)
HAMPEL	99	PL B447 127	W. Hampel *et al.*	(GALLEX Collab.)
AMBROSIO	98	PL B434 451	M. Ambrosio *et al.*	(MACRO Collab.)
APOLLONIO	98	PL B420 397	M. Apollonio *et al.*	(CHOOZ Collab.)
ATHANASSO...	98	PRL 81 1774	C. Athanassopoulos *et al.*	(LSND Collab.)
ATHANASSO...	98B	PR C58 2489	C. Athanassopoulos *et al.*	(LSND Collab.)
CLEVELAND	98	APJ 496 505	B.T. Cleveland *et al.*	(Homestake Collab.)
FELDMAN	98	PR D57 3873	G.J. Feldman, R.D. Cousins	
FUKUDA	98C	PRL 81 1562	Y. Fukuda *et al.*	(Super-Kamiokande Collab.)
HATAKEYAMA	98	PRL 81 2016	S. Hatakeyama *et al.*	(Kamiokande Collab.)
CLARK	97	PRL 79 345	R. Clark *et al.*	(IMB Collab.)
ROMOSAN	97	PRL 78 2912	A. Romosan *et al.*	(CCFR Collab.)
ATHANASSO...	96	PR C54 2685	C. Athanassopoulos *et al.*	(LSND Collab.)
ATHANASSO...	96B	PRL 77 3082	C. Athanassopoulos *et al.*	(LSND Collab.)
FUKUDA	96	PRL 77 1683	Y. Fukuda *et al.*	(Kamiokande Collab.)
FUKUDA	96B	PL B388 397	Y. Fukuda *et al.*	(Kamiokande Collab.)
GREENWOOD	96	PR D53 6054	Z.D. Greenwood *et al.*	(UCI, SVR, SCUC)
HAMPEL	96	PL B388 384	W. Hampel *et al.*	(GALLEX Collab.)
LOVERRE	96	PL B370 156	P.F. Loverre	
ACHKAR	95	NP B434 503	B. Achkar *et al.*	(SING, SACLD, CPPM, CDEF+)
AHLEN	95	PL B357 481	S.P. Ahlen *et al.*	(MACRO Collab.)
ATHANASSO...	95	PRL 75 2650	C. Athanassopoulos *et al.*	(LSND Collab.)
DAUM	95	ZPHY C66 417	K. Daum *et al.*	(FREJUS Collab.)
HILL	95	PRL 75 2654	J.E. Hill	(PENN)
MCFARLAND	95	PRL 75 3993	K.S. McFarland *et al.*	(CCFR Collab.)
DECLAIS	94	PL B338 383	Y. Declais *et al.*	
FUKUDA	94	PL B335 237	Y. Fukuda *et al.*	(Kamiokande Collab.)
VILAIN	94C	ZPHY C64 539	P. Vilain *et al.*	(CHARM II Collab.)
FREEDMAN	93	PR D47 811	S.J. Freedman *et al.*	(LAMPF E645 Collab.)
BECKER-SZ...	92B	PR D46 3720	R.A. Becker-Szendy *et al.*	(IMB Collab.)
BEIER	92	PL B283 446	E.W. Beier *et al.*	(KAM2 Collab.)
Also		PTRSL A346 63	E.W. Beier, E.D. Frank	(PENN)
BORODOV...	92	PRL 68 274	L. Borodovsky *et al.*	(COLU, JHU, ILL)
HIRATA	92	PL B280 146	K.S. Hirata *et al.*	(Kamiokande II Collab.)
CASPER	91	PRL 66 2561	D. Casper *et al.*	(IMB Collab.)
HIRATA	91	PRL 66 9	K.S. Hirata *et al.*	(Kamiokande II Collab.)
KUVSHINN...	91	JETPL 54 253	A.A. Kuvshinnikov *et al.*	(KIAE)
BERGER	90B	PL B245 305	C. Berger *et al.*	(FREJUS Collab.)
HIRATA	90	PRL 65 1297	K.S. Hirata *et al.*	(Kamiokande II Collab.)
AGLIETTA	89	EPL 8 611	M. Aglietta *et al.*	(FREJUS Collab.)
DAVIS	89	ARNPS 39 467	R. Davis, A.K. Mann, L. Wolfenstein	(BNL, PENN+)
OYAMA	89	PR D39 1481	Y. Oyama *et al.*	(Kamiokande II Collab.)
BIONTA	88	PR D38 768	R.M. Bionta *et al.*	(IMB Collab.)
DURKIN	88	PRL 61 1811	L.S. Durkin *et al.*	(OSU, ANL, CIT+)
ABRAMOWICZ	86	PRL 57 298	H. Abramowicz *et al.*	(CDHS Collab.)

ALLABY	86	PL B177 446	J.V. Allaby *et al.*	(CHARM Collab.)
ANGELINI	86	PL B179 307	C. Angelini *et al.*	(PISA, ATHU, PADO+)
VUILLEUMIER	82	PL 114B 298	J.L. Vuilleumier *et al.*	(CIT, SIN, MUNI)
BOLIEV	81	SJNP 34 787 Translated from YAF 34 1418.	M.M. Boliev *et al.*	(INRM)
KWON	81	PR D24 1097	H. Kwon *et al.*	(CIT, ISNG, MUNI)
BOEHM	80	PL 97B 310	F. Boehm *et al.*	(ILLG, CIT, ISNG, MUNI)
CROUCH	78	PR D18 2239	M.F. Crouch *et al.*	(CASE, UCI, WITW)